A CYLINDRICAL WAVEGUIDE RESONATOR FOR THE INVESTIGATION OF CERAMIC BREAKDOWN AT MICROWAVE FREQUENCIES

by

FREDERICK STEPHEN CHUTE

B.A.Sc., University of British Columbia, 1962

A THESIS SUBMITTED IN PARTIAL FULFILMENT OF THE REQUIREMENTS FOR THE DEGREE OF

MASTER OF APPLIED SCIENCE

in the Department of

Electrical Engineering

We accept this thesis as conforming to the standards required from candidates for the degree of Master of Applied Science

Members of the Department
of Electrical Engineering

THE UNIVERSITY OF BRITISH COLUMBIA

December 1963

In presenting this thesis in partial fulfilment of the requirements for an advanced degree at the University of British Columbia, I agree that the Library shall make it freely available for reference and study. I further agree that permission for extensive copying of this thesis for scholarly purposes may be granted by the Head of my Department or by his representatives. It is understood that copying or publication of this thesis for financial gain shall not be allowed without my written permission.

Department of ELECTRICAL ENGINEERING

The University of British Columbia,
Vancouver 8, Canada.

Date 6 Jan. 64

ABSTRACT

The design and construction of a microwave cavity, to be used in testing the electrical breakdown properties of titania ceramic, is described. The cavity is formed from cylindrical waveguide with a disc of titania centrally located in the cavity. Dimensions are so chosen that resonance is obtained in the H_{01} mode at 3000 mcs.

The cavity fields are derived and from them the theoretical cavity Q is found. Experimental values of Q are obtained from low power impedance measurements.

Bethe's small-hole coupling theory is applied to the design of an iris to couple power to the cavity from the waveguide system.

The dynamics of electrons in this test cavity are investigated. Time-averaged trajectories and upper limits to electron energies are derived from the Hamiltonian of the motion. With this information, the significance of electron bombardment and multipactor effects, in the ceramic breakdown, is discussed.

The cavity is used to test glazed and unglazed titania ceramic specimens at high field strengths, using a 2Mw magnetron. In addition, the effectiveness of an aluminum-titania seal on the disc edge is investigated.

It is found that, if suitable precautions are taken, the surface breakdown strength of titania is in

excess of 50 $\frac{Kv}{cm}$ when subjected to a purely tangential E field.

ACKNOWLEDGEMENT

The author wishes to express his thanks to Dr. G. B. Walker, the supervisor of this project, for many hours of valuable discussion and for his unfailing encouragement.

To Dr. R. Hayes, Mr. R. Stockwell, Dr. C. Englefield, Mr. C. R. James, and many other colleagues, the author extends his sincere appreciation.

Acknowledgement is gratefully given to the National Research Council for the assistance received from a Bursary awarded in 1962, a studentship awarded in 1963 and funds for research through the Departmental Block Term Grant.

TABLE OF CONTENTS

LIST OF ILLUSTRATIONS

A CYLINDRICAL WAVEGUIDE RESONATOR FOR THE INVESTIGATION OF CERAMIC BREAKDOWN AT MICROWAVE FREQUENCIES

1. INTRODUCTION

1.1 Brief Summary of Breakdown at Ceramic Surfaces.

Microwave tubes and more recently dielectric loaded slow wave structures make extensive use of dielectric materials. In many applications it has been found that breakdown of these dielectrics has been the limiting factor on the power handling capabilities of the devices. Failure of ceramics at microwave frequencies has been under investigation by groups at Stanford University[1,2], Sperry Gyroscope Co.[3], Electric and Musical Industries Ltd.[4], Eitel-McCullough Inc.[5], and a number of other centres.

Ceramics fail in a variety of ways. The most common types of failure are:

(a) A puncture through the material.

(b) Structural damage resulting from thermal shock.

(c) Surface sparking.

In all the investigations associated with the present study, type (c) is the principal source of breakdown. This form of ceramic failure will be referred to as surface breakdown and it appears to be critically

dependent on such factors as surface condition, contamination, metal-dielectric contacts and material composition.

1.2 Investigations Leading to Present Study.

The present experiments were originated to investigate dielectric failures observed during work on dielectric loaded periodic structures at Queen Mary College, University of London. The breakdown resulted in radial tracks of a tree-like pattern on the dielectric surface. In addition there was a light brown discoloration on the interior metal walls and on the surfaces of the dielectric discs. These loading discs were composed of a sintered ceramic consisting of titanium dioxide, with small amounts of additional compounds to improve stability. Samples were obtained from Dr. E. Schaefer, The Laboratory, 30 Thompson's Lane, Cambridge, England.

Initial experimentation showed that the breakdown strength of titania can begreatly increased by coating the ceramic with a lead borate glaze[6]. This glaze was obtained from Blythe Colour Works Ltd., Cresswell, Stoke-on-Trent, as a suspension of fine particles in water. It was sprayed on the ceramic and heated to 425°C to provide the glazed surface.

Further investigation was carried out at the

University of British Columbia[7,8,9,10]. The object was to determine what properties of the glaze were responsible for the improvement in breakdown strength. To this end, tests were made of the surface conductivity and secondary emission of both the titania ceramic and the lead borate glaze. As a result of these tests, it was concluded that differences in surface conductivities and secondary emission were not responsible for the improved breakdown properties.

Additional clarification of the breakdown process was obtained from experiments with static and dynamic fields. Plain titania was shown to suffer a permanent damage at the instant sparking occurs. Breakdown tracks, consisting of a lower semiconducting oxide, are formed by the intense local heating associated with the electrical discharges and, once formed, these tracks permanently destroy the insulation properties of the surface. Application of the thin glaze coating appears to form a protective layer on the titania surface that prevents the formation of the semiconducting oxide. As a result, initial random sparking, occasioned by surface contamination, is not permanently damaging. A spark conditioning process takes place and the breakdown threshold then rises to a much higher value.

In the majority of cases, the breakdown patterns originated at a metal-ceramic contact. Inspection of the

contact usually revealed that the metal and ceramic did not fit evenly at the point. It was concluded that the breakdown was initiated by field emission in the gaps formed at the improper metal-ceramic contact. Attempts to eliminate this edge breakdown by silvering the ceramic edge failed at microwave frequencies but had some success at d.c.

This failure of the metal-titania seal prevented adequate testing of the surface breakdown strength of the lead borate glazed discs at microwave frequencies.

1.3 Object of Present Work.

The problems associated with the edge breakdown prompted the investigation of a cylindrical S-Band cavity operating in a mode with zero E field at the outer circumference, for the purpose of eliminating metal-ceramic failures. Such a mode is the H_{01} in a cylindrical waveguide, since the E field consists only of an E_θ component.

The remainder of this thesis is concerned with the design and alignment of the H_{01} cavity and the further testing of glazed and unglazed titania discs. In addition, an assessment is made of the part played by energetic free electrons in the breakdown in this cavity.

The breakdown experiments will include tests on the effectiveness of an aluminum-titania seal in preference to the silver coating that failed in previous experimental work.

2. CAVITY DESIGN AND TESTING

2.1 Introduction.

The first experimental cavity consisted of a cylindrical waveguide cavity with a titania disc centrally located. The ceramic was held in a copper ring shrunk onto the outer edge. Dimensions were chosen so that the cavity was resonant in the H_{01} mode at 3000 mcs. The cavity diameter was dictated by the diameter of available dielectric discs to be 7.70 cm, and hence, the H_{01} mode was cutoff in the air section of the cavity. Resonance was obtained with a disc thickness of 0.582 cm. The cavity was coupled, through one end-wall, to the narrow side of the waveguide run. The side coupling proved very unsatisfactory and this small cavity was abandoned temporarily.

The problem of coupling power to a cavity in the H_{01} mode was further investigated using a 5 inch diameter cavity with no ceramic disc. In this case power was coupled to the cavity, from the end of the waveguide run, through a circular iris in one end-wall. This coupling end-wall was constructed as a removable plate thus facilitating the rapid changing of iris dimensions. The coupling was extremely erratic and repeatable results could not be obtained. Since slight variations in pressure on the bolts supporting the coupling plate

caused large fluctuations in the VSWR in the input waveguide, a mechanically rigid coupling plate was constructed. This modification was accomplished by brazing the brass coupling plate over the end of the waveguide. Consistent measurements were then obtained.

Another problem arose due to the simultaneous excitation of the E_{11} mode as well as the desired H_{01} mode. The introduction of a probe into the cavity affected the coupling, apparently as the result of mode converting. A non-conducting washer was fitted between the cylindrical walls and the end plates of the cavity, thus damping the E_{11} mode.

Using the solid coupling plate and the E_{11} mode filter, the input VSWR was reduced below 3.0 at resonance.

At this point, because of the encouraging results with the larger cavity, end coupling was adapted to the small cutoff cavity. In this case the E_{11} mode is not excited at the same frequency as the H_{01} because of the presence of the loading disc. The frequency separation was sufficient to eliminate the need for the E_{11} mode filter.

The coupling was an immediate success, with values of VSWR less than 2.5, at resonance. Figures 2.1, 2.2, and 2.3 illustrate the physical layout of this cavity.

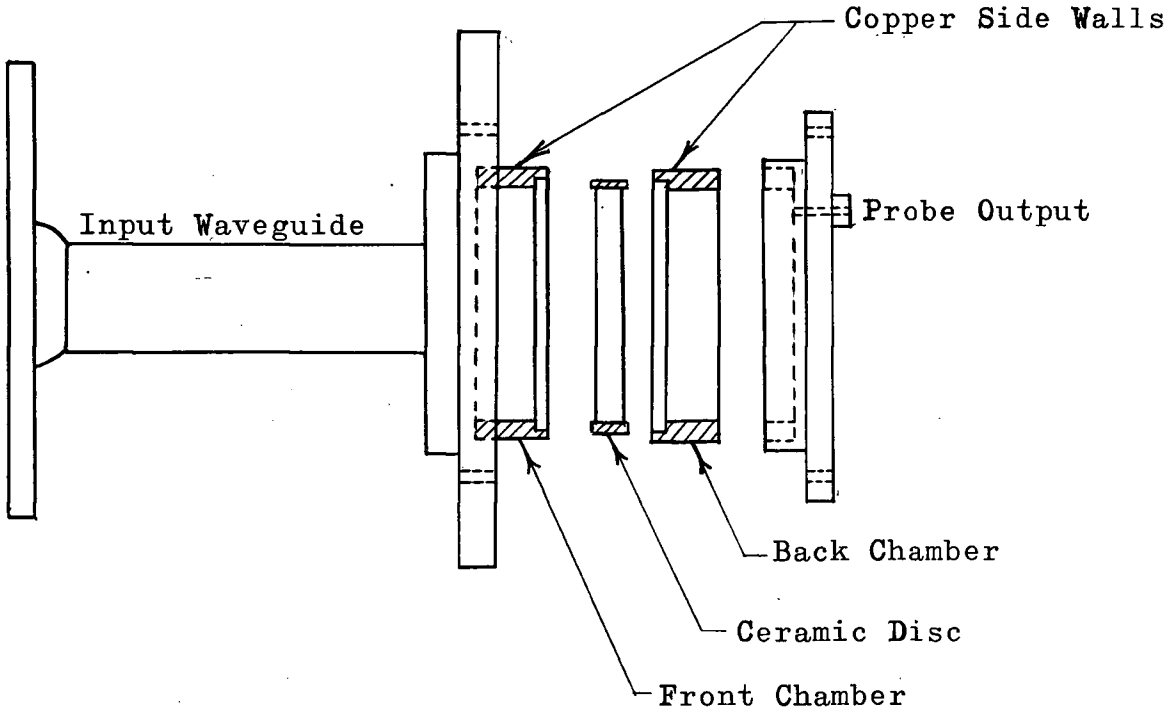

Fig. 2.1 Cross Section of S-Band Cavity

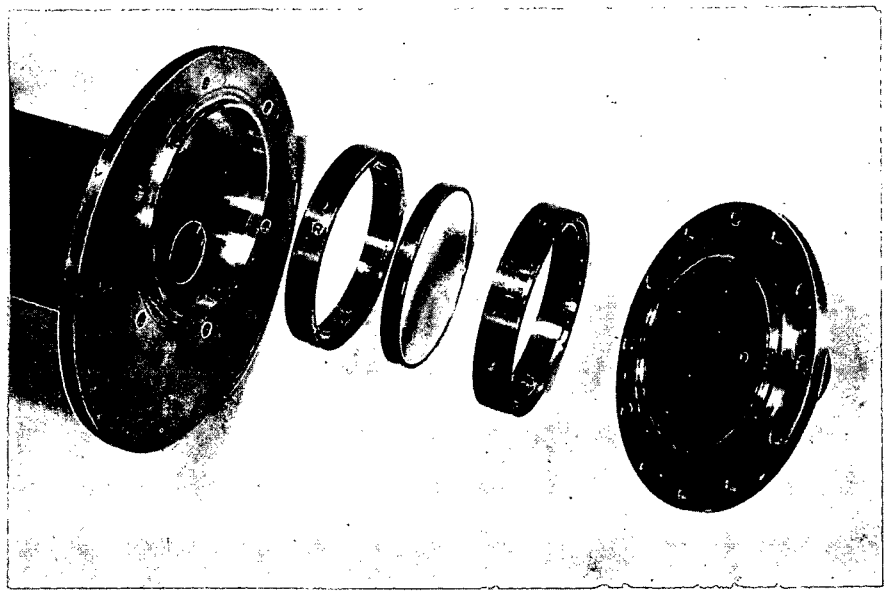

Fig. 2.2 Cavity Layout

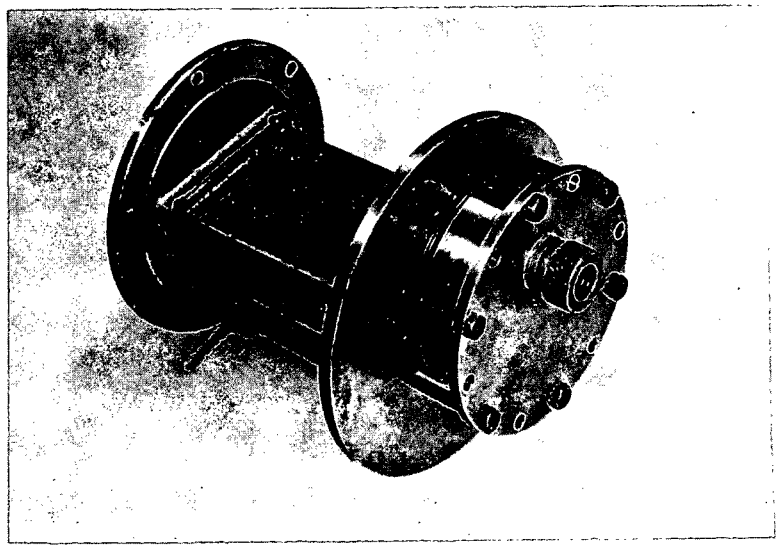

Fig. 2.3 Cavity Assembly

The remainder of this section is devoted to the design and low power testing of this cutoff cavity. The physical dimensions and theoretical unloaded Q (Q_o) are calculated. Also, the coupling hole size, experimentally obtained, is compared with the diameter given by Bethe's small-hole coupling theory.

2.2 Cavity Fields - Matching Condition and Cavity Parameters.

The cavity is designed to operate in the H_{01} mode at 3000 mcs, with the ceramic disc centrally located. The fields are so chosen that the centre of the disc and both end walls are nodal planes of the transverse E field.

The waveguide field in cylindrical coordinates is:[11]

$$H_z = H_o J_o(kr) e^{j\omega t - \gamma z}$$

$$H_r = \frac{\gamma}{k} H_o J_1(kr) e^{j\omega t - \gamma z} \qquad \ldots 2.1$$

$$E_\theta = \frac{-j\omega\mu}{k} H_o J_1(kr) e^{j\omega t - \gamma z}$$

assuming perfectly conducting metal walls and lossless dielectric. γ is the complex propagation constant and

$$\gamma^2 = k^2 - \omega^2\mu\varepsilon \qquad \ldots 2.2$$

The addition of two travelling waves of the form given by equations 2.1 yields the H_{01} field for an empty cavity. Thus with z = o a nodal plane, the H_{01} cavity field becomes:

$$H_z = -H_1 J_o(kr)\sinh \gamma z \cdot e^{j\omega t}$$

$$H_r = \frac{\gamma}{k} H_1 J_1(kr)\cosh \gamma z \cdot e^{j\omega t} \qquad \ldots 2.3$$

$$E_\theta = \frac{\pm j\omega\mu}{k} H_1 J_1(kr)\sinh \gamma z \cdot e^{j\omega t}$$

The radius of the cavity is fixed, by the diameter of available ceramic discs, at a = 3.85 cm. In order to satisfy the boundary conditions, E_θ must be zero at r = a. For the H_{01} mode this constraint requires that ka is the first zero of $J_1(kr)$. Hence, ka = 3.83 and k = 99.5. Thus, from equation 2.2, $\gamma = j\beta = j598$ in the dielectric region and $\gamma = \alpha = 77.2$ in the air region. The fields outside the dielectric disc are, therefore, expressed in terms of hyperbolic functions while those within the disc are represented by trigonometric functions.

The field pattern in the dielectric loaded cavity can be obtained by considering standing waves, of the form given by equations 2.3, to exist in both the air and dielectric portions of the cavity. By matching field

components at the dielectric-air interface, it is possible to relate α and β to the physical dimensions of the cavity. To simplify the expressions, different $z = o$ planes are chosen in each section. Figure 2.4 shows a cross-sectional view of the cavity with these origins marked.

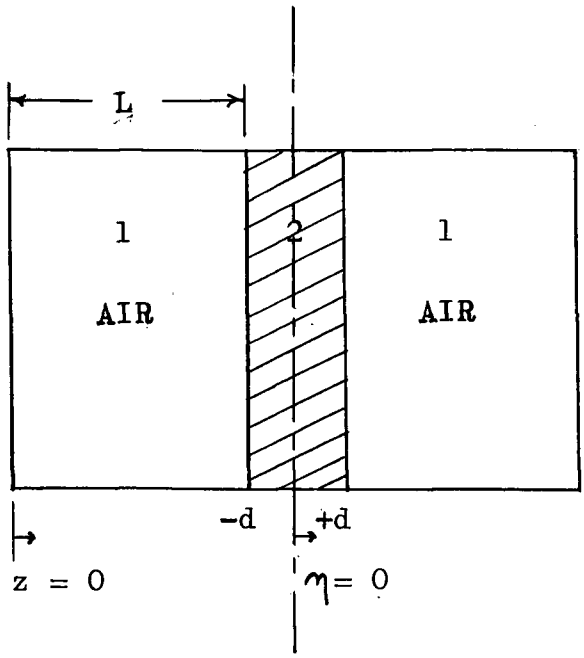

Fig. 2.4 Cavity Schematic

The appropriate fields are:

(a) In the air section

$$H_z = -H_1 J_o(kr)\sinh \alpha z \cdot e^{j\omega t}$$

$$H_r = \frac{\alpha}{k} H_1 J_1(kr)\cosh \alpha z \cdot e^{j\omega t} \quad \ldots 2.4$$

$$E_\theta = \frac{j\omega\mu_1}{k} H_1 J_1(kr)\sinh \alpha z \cdot e^{j\omega t}$$

(b) In the dielectric section

$$H_z = H_2 J_o(kr)\sin\beta\eta \cdot e^{j\omega t}$$

$$H_r = \frac{-\beta}{k} H_2 J_1(kr)\cos\beta\eta \cdot e^{j\omega t} \quad \ldots 2.5$$

$$E_\theta = \frac{-j\omega\mu_2}{k} H_2 J_1(kr)\sin\beta\eta \cdot e^{j\omega t}$$

At the dielectric-air interface the following boundary conditions must be satisfied:

(a) $H_{\text{tangent-air}} = H_{\text{tangent-dielectric}}$

(b) $E_{\text{tangent-air}} = E_{\text{tangent-dielectric}}$ ...2.6

(c) $\mu_1 H_{\text{normal-air}} = \mu_2 H_{\text{normal-dielectric}}$

Thus

$$H_1\mu_1 \sinh\alpha L = H_2\mu_2 \sin\beta d$$

$$H_1\alpha \cosh\alpha L = -H_2\beta \cos\beta d$$

Dividing these two equations yields the matching condition:

$$\tanh\alpha L \cdot \cos\beta d = \frac{-\mu_2}{\mu_1} \cdot \frac{\alpha}{\beta} \qquad \ldots 2.7$$

If d is to give a practical disc thickness, βd must lie between $\frac{\pi}{2}$ and π. To make the most efficient use of available power it is desirable to have a maximum E_θ field at the disc surface. This condition implies that βd must approximately equal $\frac{\pi}{2}$, but then αL must approach infinity to satisfy equation 2.7. The larger αL becomes, the more difficult it is to couple power to the cavity. A satisfactory compromise is $\alpha L = 1$. Hence, from the matching condition, the cavity parameters are:

Cavity Length (2L + 2d)	0.0317 meter
Cavity Radius (a)	0.0385 meter
Disc Thickness (2d)	0.00582 meter
α	77.2 nepers meter
β	598 radians meter
Characteristic Number (k)	99.5
Relative Permittivity (ε_r) of titania disc	93

2.3 Design of Coupling Aperture.

Power is coupled to the cavity from the end of the waveguide through a circular iris in one of the cavity end walls. Figure 2.5 illustrates the fashion in which coupling is obtained.

F. Shnurer[12], using the small hole coupling theory developed by Bethe[13], has related the coupling hole diameter to the loaded Q (Q_L) of a cavity. Shnurer proceeds by setting

$$Q_L = \frac{\omega \times \text{stored energy}}{S}$$

where S is the power lost through a coupling hole in a cavity coupled to a waveguide system. It is felt that this expression is in error in neglecting the wall loss of the cavity.

Consider a cavity coupled to a waveguide system by a lossless window. It can be shown that Q_L defines the rate at which this cavity loses energy in the absence of excitation. This energy loss is comprised of the wall loss plus the energy radiated through the coupling hole, in other words $P_w + S$. For unity coupling $P_w = S$ and the expression for Q_L should be:

$$Q_L = \frac{\omega \times \text{stored energy}}{P_w + S} = \frac{\omega \times \text{stored energy}}{2S}$$

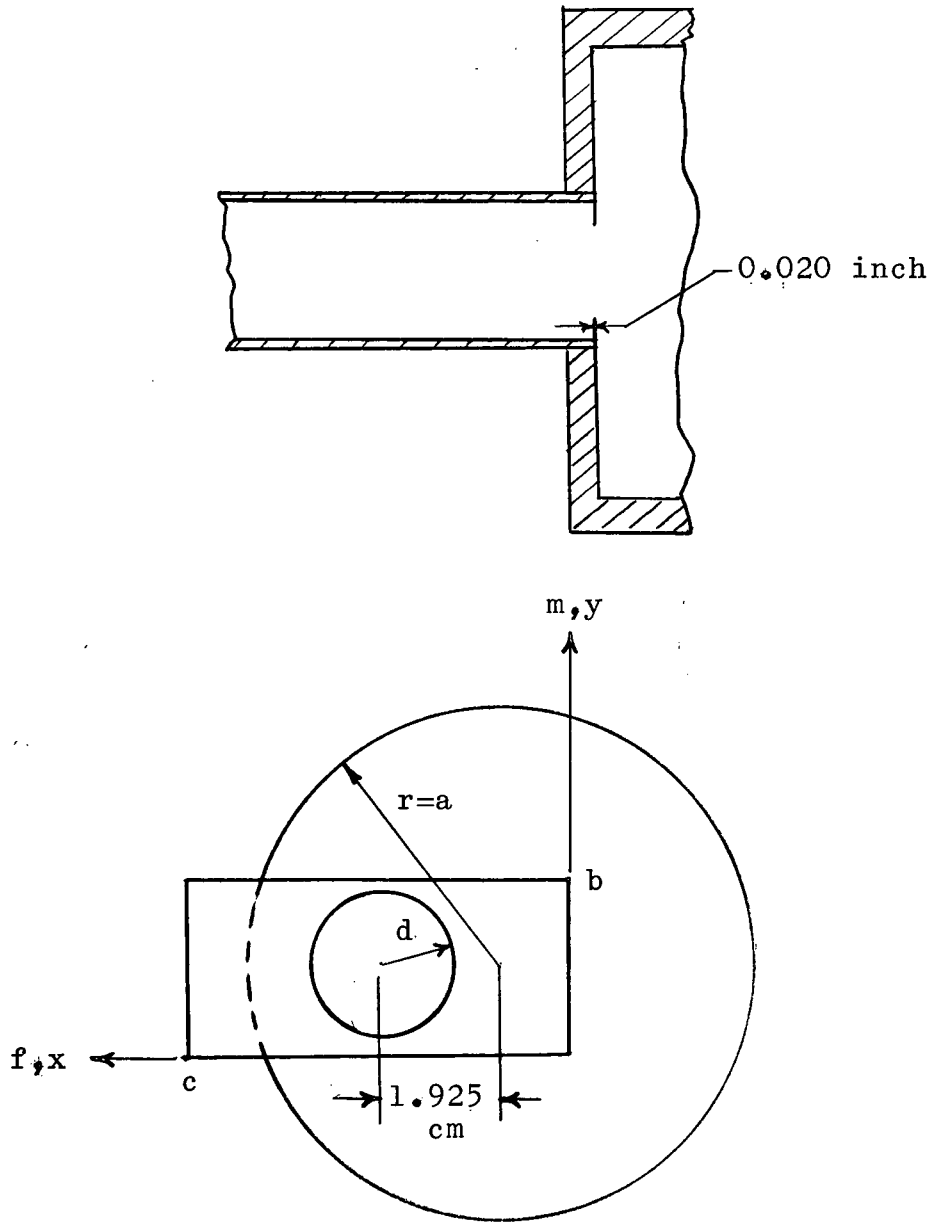

Fig. 2.5 Coupling Configuration

In the following calculations the modified value of Q_L will be used but the method will be the same as outlined by Shnurer.

Bethe has shown that the power lost, through a window in a cavity, into the end of a waveguide can be expressed as:

$$S = \frac{k_o^2}{Sa}\left|PE_{on}E_{an} + jM_1H_{of}H_{af} + jM_2H_{om}H_{am}\right|^2 \quad \ldots 2.8$$

where P, M_1, M_2, are dependent on window geometry and are known as polarizabilities. The fields with subscript "o" are cavity fields, those with subscript "a" are waveguide fields. The subscripts f, m, n, refer to the axes of the window. Sa is a normalizing constant. Here $P = \frac{d^3\eta}{12}$, $M_1 = M_2 = \frac{d^3\eta}{6}$, where $\eta = \sqrt{\frac{\mu}{\varepsilon}}$, $k_o = \frac{2\pi}{\lambda_o}$, and d is the iris diameter.

The dominant mode fields in the rectangular guide are:[14]

$$H_z = H_2 \cos \frac{\pi x}{c} \cdot e^{j(\omega t - \beta_o z)}$$

$$H_x = \frac{j2c}{\lambda_g} H_2 \sin \frac{\pi x}{c} \cdot e^{j(\omega t - \beta_o z)} \quad \ldots 2.9$$

$$E_y = \frac{-j2c}{\lambda_o} \eta H_2 \sin \frac{\pi x}{c} \cdot e^{j(\omega t - \beta_o z)}$$

The coupling fields involved in this case are those fields

in the cavity and the waveguide at z = o, x = $\frac{c}{2}$, and r = 1.925 cm.

Hence

$$S = \frac{k_o^2}{Sa} \left| jM_1 H_r H_x \right|^2$$

$$H_r = \frac{\alpha}{k} H_1 J_1(kr)$$

$$H_x = \frac{j2c}{\lambda_g} H_2$$

Therefore

$$S = \frac{k_o^2}{Sa} \left| \frac{jd^3\eta}{6} \cdot \frac{\alpha}{k} H_1 J_1(kr) \cdot \frac{j2c}{\lambda_g} H_2 \right|^2 \qquad \ldots 2.10$$

But from Bethe $Sa = \int \text{Real}(E_T \times H_T^*) ds$ where, in this case, E_T and H_T are the transverse waveguide fields.

$$Sa = \frac{-j2c}{\lambda_o} \eta H_2 \frac{j2c}{\lambda_g} H_2 \int_o^b \int_o^c \sin^2 \frac{\pi x}{c} \, dxdy$$

$$= \frac{4c^2 \eta H_2^2}{\lambda_o \lambda_g} \cdot \frac{c}{2} \cdot b = \frac{2c^3 b \eta H_2^2}{\lambda_o \lambda_g} \qquad \ldots 2.11$$

Thus, substituting $J_1^2(k \cdot 1.925) = (.5807)^2$

$$S = \frac{0.440 H_1^2 d^6 \eta}{\lambda_o \lambda_g c b} \qquad \ldots 2.12$$

and

$$Q_L = \frac{\omega \times \text{energy stored}}{2S} \qquad \ldots 2.13$$

The stored energy is calculated in section 2.4 and is given as $81,380 \times 10^{-15} H_1^2$ joules.

Hence

$$Q_L = \frac{0.348 \lambda_g cb}{2d^6 \eta}$$

and

$$d^6 = \frac{0.348 \lambda_g cb}{2\eta Q_L} \qquad \ldots 2.14$$

For the critically coupled case $Q_L = \frac{Q_o}{2}$. Q_o is given in section 2.4 as 2850.

Therefore

$$Q_L = 1425 \text{ and } \lambda_g = \frac{\lambda_o}{\left[1 - \left(\frac{\lambda_o}{2c}\right)^2\right]^{\frac{1}{2}}} = 13.9 \text{ cm}$$

also c = 7.2 cm and b = 3.4 cm. $\eta = 377$.

Hence

$$d^6 \approx 1.1 \times 10^{-10} \text{ m}^6$$

and

$$d \approx 2.18 \text{ cm}$$

Experimentally it was found that an input standing wave ratio of less than 2.0 could be obtained with a hole diameter of 2.60 cm. Thus, the theoretical diameter derived above is less than 15 percent in error. The deviation can be attributed partly to the fact that the maximum Q_o was used in the calculations and not the actual

Q_o which is much lower. Using the actual Q_o will lead to a larger diameter. Also it must be remembered that Bethe made the approximation that $d \ll \lambda_o$. The useable accuracy achieved in calculating coupling holes in the above fashion, however, indicates that Bethe's small-hole theory provides a satisfactory approximation for holes of the order of $\frac{\lambda_o}{4}$ in diameter. This same observation was made by Shnurer in his work on aperture-coupled filters.

2.4 Theoretical Unloaded Q of Disc Loaded Resonator.

The unloaded Q of a cavity is given by

$$Q_o = \frac{\omega \times \text{stored energy}}{\text{mean power dissipated}} \qquad \ldots 2.15$$

The stored energy, ε_s, is:

$$\varepsilon_s = \frac{1}{2} \int_{vol} \left[\frac{1}{2} \varepsilon |E|^2 + \frac{1}{2} \mu |H|^2 \right] dv$$

and since for the lossless cavity

$$\int_V \frac{1}{2} \varepsilon |E|^2 \, dv = \int_V \frac{1}{2} \mu |H|^2 dv$$

$$\varepsilon_s \cong \frac{1}{2} \int_{vol} \varepsilon |E|^2 \, dv$$

The complete ε_s consists of two portions; the energy stored

in the dielectric region and the energy stored in the air space.

In the air space:

$$\varepsilon_s = 2 \times \frac{1}{2} \frac{\omega^2 \mu_1^2}{k^2} \varepsilon_2 \pi H_1^2 \int_0^a 2rJ_1^2(kr)dr \int_0^L \sinh^2 \alpha z dz$$

$$= 2 \times \frac{\pi \varepsilon_1}{k^2} \omega^2 \mu_1^2 H_1^2 \cdot \frac{a^2}{2} J_o^2(ka) \cdot 5.26 \times 10^{-3}$$

$$= 1984 \times 10^{-15} H_1^2 \text{ joules} \qquad \ldots 2.16$$

In the dielectric region:

$$\varepsilon_s = 2 \times \frac{1}{2} \frac{\omega^2 \mu_2^2}{k^2} \varepsilon_2 2\pi H_2^2 a^2 \frac{J_o^2}{2}(ka) \int_0^d \sin^2 \beta \eta d\eta$$

$$\varepsilon_s = 56{,}000 \times 10^{-15} H_2^2$$

and from equation 2.6, $H_1 = 0.84 H_2$.

Therefore

$$\varepsilon_s = 79{,}400 \times 10^{-15} H_1^2 \text{ joules} \qquad \ldots 2.17$$

A good approximation of the wall loss in the cavity can be made by using the value of H_T at the wall and the wave impedance of the wall.

Then

$$P = \frac{1}{2}\frac{1}{\Delta g}\int |H_T|^2 \, ds$$

where Δ is the skin depth and is given as $\Delta = \left(\frac{2}{\omega\mu g}\right)^{\frac{1}{2}}$.

g is the conductivity of the wall.

The power lost to the brass end walls is:

$$P_1 = \frac{1}{2}\frac{1}{\Delta g}\int_0^a \int_0^{2\pi} \frac{\alpha^2}{k^2} H_1^2 J_1^2(kr) ds \times 2$$

$$= \frac{\alpha^2 \pi}{\Delta g k^2} H_1^2 \cdot \frac{a^2}{2} J_o^2(ka) \times 2$$

$$= 12.72 \times 10^{-6} H_1^2 \text{ watts} \qquad \ldots 2.18$$

The power lost to the copper side walls in the dielectric portion is:

$$P_2 = \frac{\pi a}{\Delta g} H_2^2 J_o^2(ka) \int_0^d \sin^2 \beta\eta \cdot d\eta \times 2$$

$$= 1.27 \times 10^{-6} H_1^2 \text{ watts} \qquad \ldots 2.19$$

The power lost to the side walls in the air region is:

$$P_3 = \frac{\pi a}{\Delta g} H_1^2 J_o^2(ka) \int_0^L \sinh^2 \alpha z dz \times 2$$

$$= 2.96 \times 10^{-6} H_1^2 \text{ watts} \qquad \ldots 2.20$$

The power lost to the dielectric is given as[15]:

$$P_D = \frac{1}{2}\int_v g|E|^2 dv \qquad \ldots 2.21$$

$$= \frac{1}{2}\int_v \omega\epsilon_2 \tan\delta\,|E|^2 dv,$$

$\tan\delta \cong 0.00035$ for titania.

$$P_D = \epsilon_2 \tan\delta\omega^3\mu_2^2\pi H_2^2 J_o^2(ka)\frac{a^2}{2k^2} \times 1.59 \times 10^{-3} \times 2$$

$$= 521 \times 10^{-6} H_1^2 \text{ watts} \qquad \ldots 2.22$$

The results for the losses are:

end walls	$12.72 \times 10^{-6} H_1^2$
side walls	$1.27 \times 10^{-6} H_1^2$
.....	$2.96 \times 10^{-6} H_1^2$
dielectric	$521.0 \times 10^{-6} H_1^2$
	$538 \times 10^{-6} H_1^2$ watts

The results for the stored energy are:

dielectric region	$1984 \times 10^{-15} H_1^2$
air region	$79400 \times 10^{-15} H_1^2$
	$81400 \times 10^{-15} H_1^2$ joules

Hence from equation 2.15 the unloaded Q is:

$$Q_o = \frac{6.28 \times 10^9 \times 3 \times 81400 \times 10^{-15} H_1^2}{538 \times 10^{-6} H_1^2}$$

$$Q_o = 2850$$

2.5 A Method of Q_o Measurement.

The Q of a cavity can be obtained from a plot of VSWR, in the input waveguide, against frequency about the resonance point, using a method described by Ginzton[16]. A knowledge of the coupling is required and this is expressed in terms of a coupling coefficient, φ. φ, in turn, is easily related to the VSWR at resonance and at the half power frequencies, thus enabling Q_o to be determined directly from standing wave ratio data.

φ is defined in terms of the parameters of the resonator equivalent circuit shown in Figure 2.6. Z_o is the waveguide characteristic impedance and L_1 is the self inductance of the coupling hole. C, L, R_s are cavity parameters and M represents the coupling between the waveguide and the cavity.

Consider the impedance Z_1 coupled in series with the cavity parameters.

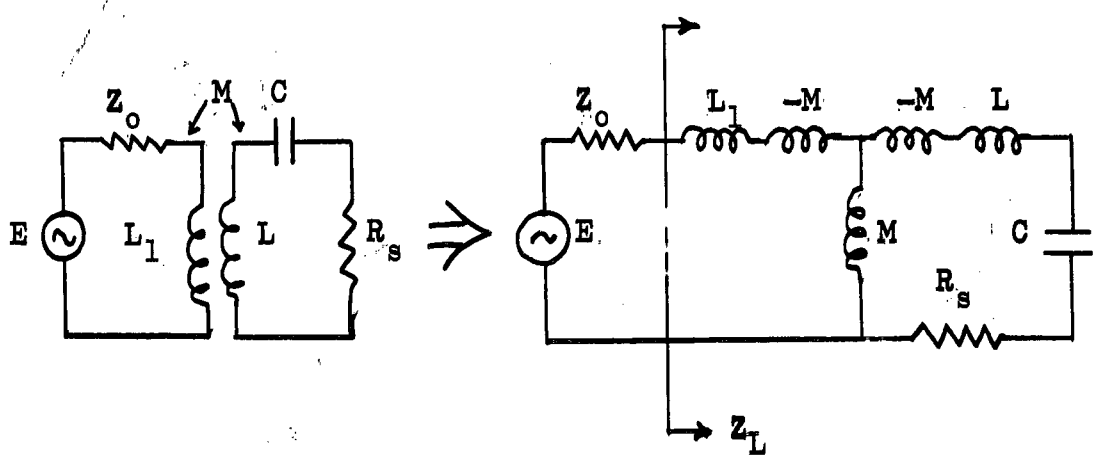

Fig. 2.6 Lumped Element Equivalent Circuit of Coupling

$$Z_1 = \frac{(\omega M)^2}{Z_o + j\omega L_1} = \frac{(\omega M)^2}{Z_o\left(1 + \left(\frac{\omega L_1}{Z_o}\right)^2\right)} \left[1 - \frac{j\omega L_1}{Z_o} \right]$$

which may be written as

$$Z_1 = \varphi R_s \left(1 - \frac{j\omega L_1}{Z_o}\right)$$

where

$$\varphi = \frac{(\omega M)^2}{Z_o R_s} \cdot \frac{1}{1 + \left(\frac{\omega L_1}{Z_o}\right)^2}$$

and

$$\frac{1}{1 + \left(\frac{\omega L_1}{Z_o}\right)^2} \cong 1$$

hence

$$\varphi \cong \frac{\omega^2 M^2}{Z_o R_s} \qquad \ldots 2.23$$

The total impedance with which the line is terminated is given as:

$$Z_L = j\omega L_1 + Z$$

where

$$Z = \frac{\omega^2 M^2}{R_s\left[1 + j(\omega L - \frac{1}{\omega C})\frac{1}{R_s}\right]}$$

$$\frac{Z_L}{Z_o} \cong \frac{j\omega L_1}{Z_o} + \frac{\varphi}{1 + j2Q_o\frac{\delta\omega}{\omega}} \qquad \ldots 2.24$$

The interpretation of the impedance expressions can be aided by choosing special reference planes, along the waveguide run, at which the term representing the self-reactance of the coupling system disappears. In general, the impedance of these planes, in terms of the load impedance , is:

$$\frac{Z_c}{Z_o} = \frac{Z_L + jZ_o \tan\beta_o l}{Z_o + jZ_L \tan\beta_o l} \qquad \ldots 2.25$$

where "l" is the distance from the load to the reference plane.

To locate such a reference plane, detune the cavity and locate a voltage node along the waveguide. This position is called the detuned-short.

At the detuned-short, with the cavity detuned, the impedance is zero and from equation 2.24 $Z_L = j\omega L_1$. Substituting these values into equation 2.25 yields:

$$\tan \beta_o l = \frac{-\omega L_1}{Z_o}$$

Thus, the impedance at the detuned short in the vicinity of resonance can be written as:

$$\frac{Z_c}{Z_o} \cong \frac{\varphi}{1 + j2Q_o\left[\frac{\delta\omega}{\omega} - \frac{\varphi\omega L_1}{2Z_o Q_o}\right]} \qquad \ldots 2.26$$

$$\frac{Z_c}{Z_o} \cong \frac{\varphi}{1 + j2Q_o(M - M_o)} \qquad \ldots 2.27$$

At certain frequencies $\frac{Z_c}{Z_o} = \frac{\varphi}{1 \pm j1}$, hence, $2Q_o(M_1 - M_o) = 1$ or $2Q_o(M_2 - M_o) = -1$.

Therefore

$$Q_o = \frac{1}{M_1 - M_2} = \frac{1}{\frac{(\omega_1 - \omega_o)}{\omega_1} - \frac{(\omega_2 - \omega_o)}{\omega_2}} \cong \frac{\omega_o}{\omega_1 - \omega_2}$$

$$\frac{\omega_o}{\omega_1 - \omega_2} = \frac{f_o}{f_1 - f_2}$$

Thus, f_1 and f_2 are the half power frequencies, from equation 2.26. At these values of frequency the impedance at the detuned short is:

$$\frac{Z_c}{Z_o} = \frac{\varphi}{1 \pm j1} \qquad \ldots 2.28$$

The corresponding value of VSWR at these frequencies can be obtained from[17]:

$$S = \frac{|Z_c + Z_o| + |Z_c - Z_o|}{|Z_c + Z_o| - |Z_c - Z_o|} \qquad \ldots 2.29$$

where S is the VSWR. Hence, the value of S at the half power frequencies is:

$$S_{\frac{1}{2}} = \frac{2 + \varphi^2 + (4 + \varphi^4)^{\frac{1}{2}}}{2\varphi} \qquad \ldots 2.30$$

φ can be found in terms of the standing wave at resonance for two distinct cases, when $\varphi > 1$ and when $\varphi < 1$. At resonance $\frac{Z_c}{Z_o} \cong \varphi$ and from 2.29:

$$\varphi > 1 \text{ (overcoupled)} \ldots\ldots \varphi = S_o$$

$$\varphi < 1 \text{ (undercoupled)} \ldots\ldots \varphi = \frac{1}{S_o}$$

where S_o is the VSWR at resonance.

The procedure for finding Q_o is as follows:

(a) Plot VSWR against frequency about resonance.

(b) Locate detuned short and bring cavity carefull to resonance.

(c) Explore the voltage distribution around the detuned short position using a slotted line section.

A voltage maximum means $\varphi = S_o$

A voltage minimum means $\varphi = \frac{1}{S_o}$

(d) Calculate $S_{\frac{1}{2}}$ and from the graph (a) find f_1 and f_2. Then $Q_o = \frac{f_o}{f_1 - f_2}$.

2.6 Low Power Test Results.

The low power test equipment was used to measure the Q_o of the cavity and to adjust the resonance as near as possible to 2998 mcs, the fixed frequency of the high power magnetron. Some slight control on the resonant frequency was needed to enable the frequency to be set to 2998 mcs each time the cavity was assembled. These small variations in the resonance point were obtained by placing thin aluminum washers between the ceramic disc and the metal side walls. The washers effectively lengthened the cavity, thereby lowering the resonant frequency.

A small amount of power was coupled out of the cavity by an H field probe and monitored. The resonant frequency was taken as the frequency at which this output power was a maximum.

Each time the cavity was assembled, prior to a high power test, the resonant frequency was set at 2998 mcs and a plot of VSWR against frequency was taken on the low power bench.

Typical graphs of VSWR versus frequency under a number of differing conditions are shown in figures 2.7, and 2.8.

Figure 2.7

The disc in this case was glazed on one side with lead borate and the disc edge was aluminized using a vacuum evaporation technique. Here, using the method of section 2.5:

$$S_o = 2$$

$$\varphi = \frac{1}{2} \text{ (undercoupled)}$$

$$S_{\frac{1}{2}} = 4.27$$

$$\Delta f = 2.56 \text{ Mc/s}$$

$$f_o \cong 2998.4 \text{ Mc/s}$$

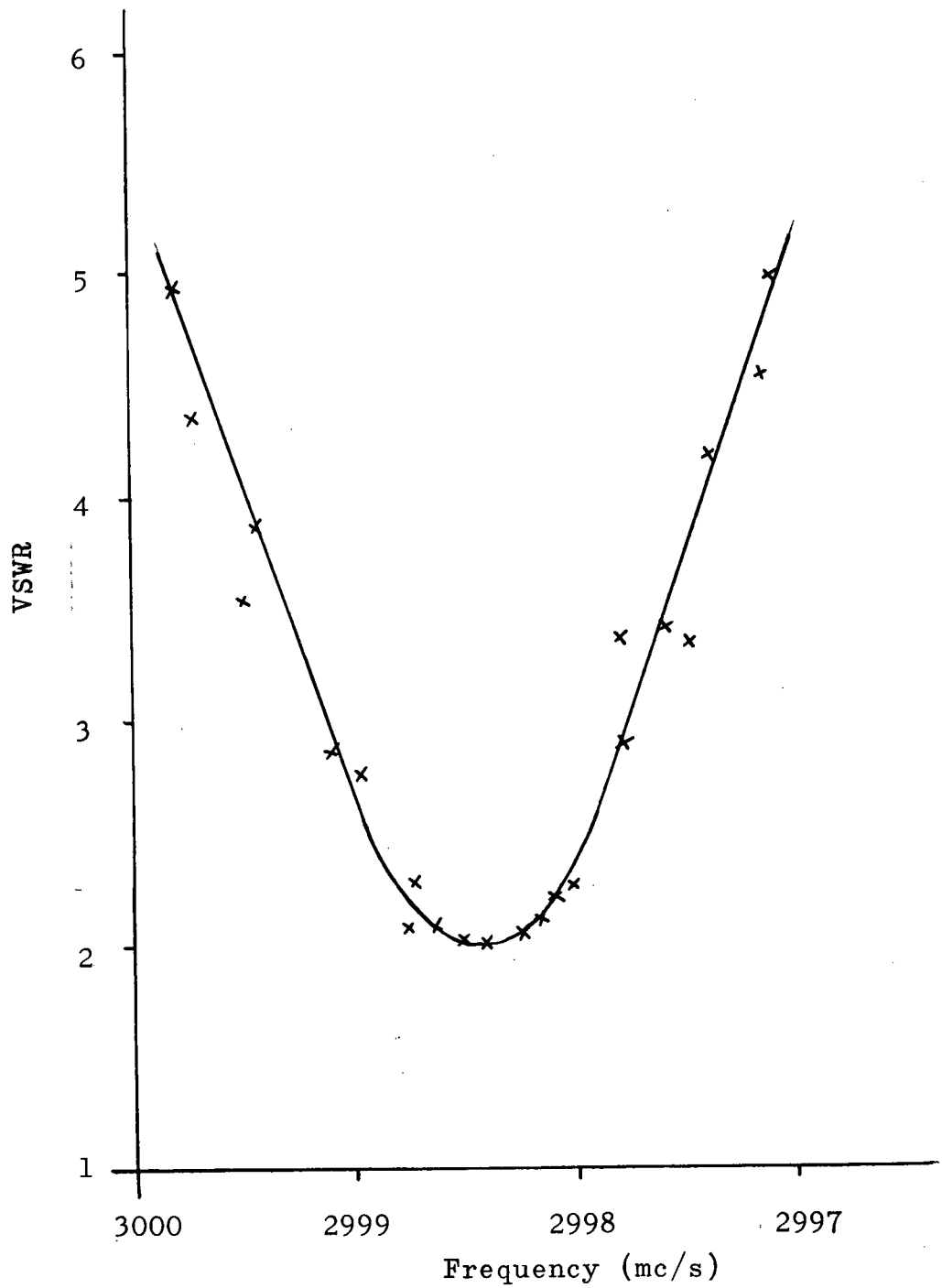

Fig. 2.7 VSWR Characteristic

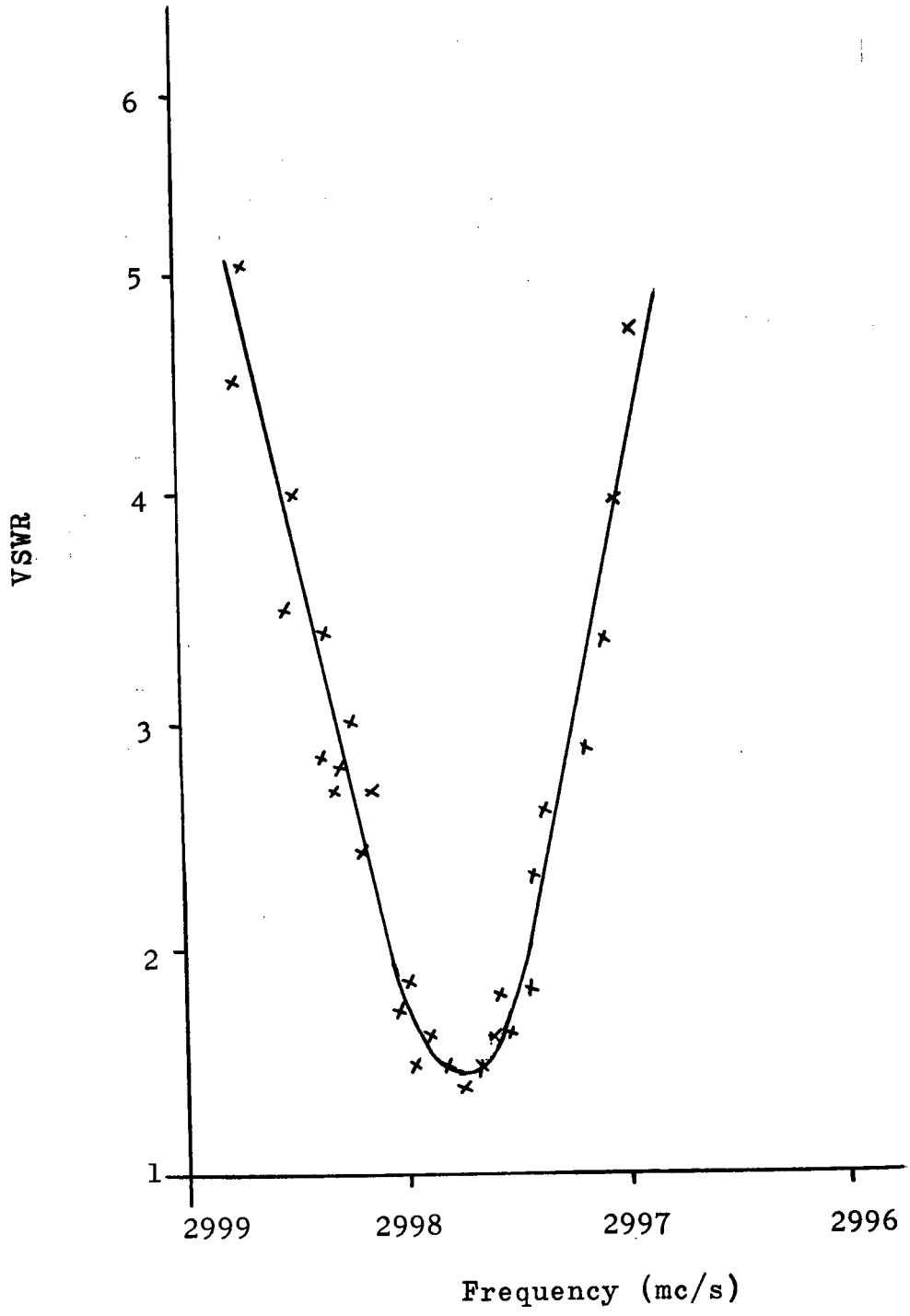

Fig. 2.8 VSWR Characteristic

and

$$Q_o = \frac{f_o}{\Delta f} \cong 1170$$

Figure 2.8

The disc had a glaze coating on one side but the edge was not aluminized. In addition, the cavity was made vacuum tight using a cylindrical brass jacket enclosing the entire cavity. Here:

$$S_o = 1.44$$

$$\varphi = 1/1.44 \text{ (undercoupled)}$$

$$S_{\frac{1}{2}} = 3.27$$

$$\Delta f = 1.57 \text{ Mc/s}$$

$$f_o = 2998.2 \text{ Mc/s}$$

and

$$Q_o = \frac{f_o}{\Delta f} \cong 1900$$

These values of Q_o are considerably below the theoretical maximum given in section 2.4. A portion of the deviation can be attributed to surface irregularities and the approximate nature of both the calculations of cavity losses and the graphical method used. The major source of error, however, is the neglect of loss associated with the thin lead borate glaze. This loss can be taken into account by the following approximation:

$$P_D = \frac{1}{2} \int_v \omega\varepsilon \tan\delta |E|^2 dv$$

where

$$|E| = \frac{\omega\mu}{k} H_1 J_1(kr) \sinh\alpha z.$$

Assume that the cavity fields are approximately constant over the glaze thickness, d.

Therefore

$$P_D \cong \pi\omega\varepsilon \tan\delta . d \int_0^a |E|^2 \, r dr$$

$$\cong \frac{\pi d \varepsilon_r \varepsilon_o \mu^2 \omega^3 \tan\delta}{k^2} \times 1.18^2 H_1^2 . \frac{a^2}{2} . J_o^2(ka)$$

Luthra[9] has determined ε_r and $\tan\delta$ for lead borate glazed on titania as $\varepsilon_r = 19.3$, $\tan\delta = 0.033$.

Hence

$$P_D \cong 81.3 \times 10^{-6} H_1^2 \text{ watts}/0.001"$$

The glaze thickness is not known exactly, but it lies between 0.001" and 0.005". If for example d = 0.003",

$$P_D \cong 244 \times 10^{-6} H_1^2 \text{ watts},$$

and

$$Q_o \cong \frac{18.85 \times 10^9 \times 81400 \times 10^{-15}}{244 + 538}$$

Therefore

$$Q_o \cong 1960$$

This value of Q_o agrees closely with the experimental data.

3. CERAMIC BREAKDOWN IN THE S-BAND CAVITY

3.1 Introduction.

Breakdown tests were carried out using a high power microwave system consisting of a 10 cm magnetron and modulator unit. Power was delivered in the form of 2μs pulses at a 60 cps recurrence frequency, and was continuously variable from a few kilowatts to a peak of 2 Mw. Although the magnetron oscillated at a fixed frequency, 2998 mcs, it was possible to tune it over a three to four megacycle range by means of a phase shifter mismatch unit and by varying the magnetron magnet current. A thermistor bridge was used to measure the power, and the frequency was monitored by a cavity wavemeter. Figure 3.1 shows the high power system.

In order to handle the power required for breakdown testing it was necessary to evacuate the waveguide system. The cavity was made vacuum tight by enclosing it in an oversized cylindrical jacket which was sealed by "O" rings to the flanges that form the cavity end plates. The probe hole was closed by an "O" ring and a small piece of glass, and it was possible to view the back chamber under vacuum conditions. The cavity was pumped through the coupling hole and waveguide run, the back chamber being evacuated through holes in the side walls. Figure 3.2 illustrates the pumping scheme. The

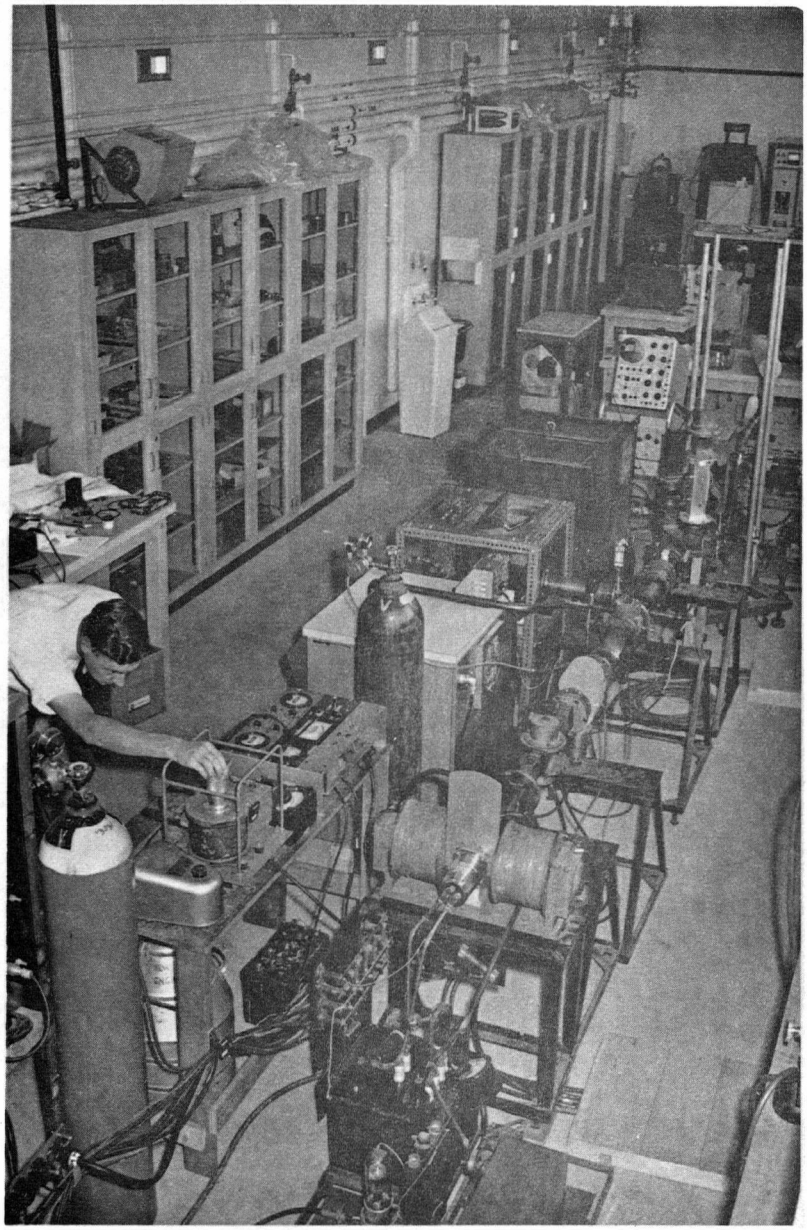

Fig. 3.1 High Power System

system was evacuated by a 3 inch mercury diffusion pump, with a liquid nitrogen trap, backed by rotary pump.

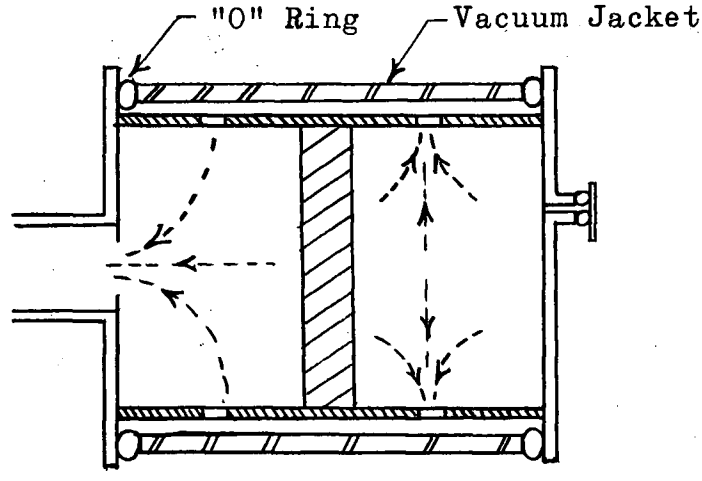

Fig. 3.2 Cavity Pumping Scheme

The following procedure was used for all the high power tests. The cavity was assembled with the ceramic disc to be tested and was placed in the vacuum jacket. Low Power measurements were made of the unloaded Q_o and the resonant frequency was set as closely as possible to

2998 mcs. The cavity was then bolted to the high power waveguide and the system was evacuated. The breakdown testing was commenced only after the pressure level, as measured on an ion guage several feet from the cavity itself, was reduced below 10^{-5} mm Hg.

Power was increased in small steps until either there was evidence of breakdown or the maximum power level was reached. Each increase in power caused a sudden pressure rise, due to outgassing of the waveguide walls. The original pressure level was rapidly restored by the diffusion pump. At each step the magnetron frequency was varied over a 3 to 4 megacycle range to ensure that power was delivered to the cavity at its resonant frequency.

3.2 Breakdown Test I and II - Unglazed Disc.

The experimental procedure for these two tests was exactly as outlined in the Introduction. In addition, a Geiger-Muller Counter was located near the cavity for the purpose of monitoring any radiation generated by energetic electrons as a result of breakdown at the ceramic disc.

The power was gradually increased to a peak of 1.2 Mw, allowing sufficient time for outgassing of the system. The Geiger Counter registered only the random radiation from the magnetron power supply and modulator

and there was no change in count when a breakdown occurred. Externally, the only sign of breakdown was the considerable increase in the temperature of the cavity.

In both tests dismantling the cavity revealed a large discoloured area on the disc surface nearest the coupling hole. This breakdown pattern appeared to be an extensive network of interlocking tracks of reduced titania. No other breakdown was evident anywhere on the disc.

The reduced region was centrally located and about 3 cm in diameter. Within this breakdown area the disc surface contained a number of pits, some about 0.1 cm deep. The majority of the tracks of reduced titania did not coincide, as in many previous experiments[10], with the E field pattern. The first test did have one large track at a radius of 1.8 cm, the position of maximum E field in the cavity.

A portion of the brass end wall, directly opposite the breakdown region, was also discoloured. The discolouration had the form of concentric rings of various colours, mainly reds and blues. The rings were concentric and circular to a high degree. There was no distortion where they intersected the coupling hole. Figure 3.3 shows the breakdown on the disc and Figure 3.4 shows the concentric rings.

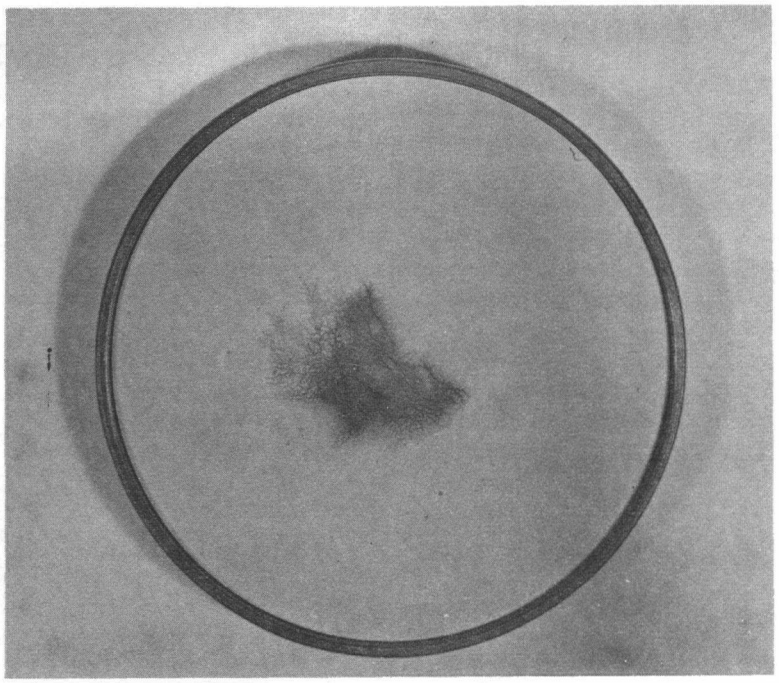

Fig. 3.3 Ceramic Breakdown-Test II

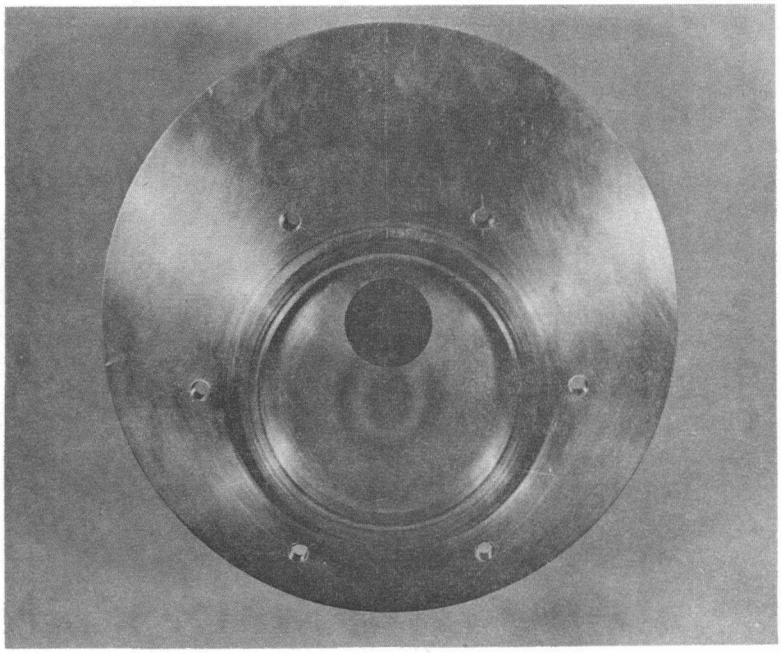

3.3 Breakdown Test III - Glazed Disc.

In an effort to eliminate the surface breakdown observed in the previous tests, the side of the disc nearest the coupling hole was sprayed with a lead borate solution. The disc was then heated to a temperature of 430°C for a glazing action to occur. This process produced a smooth glossy surface; the final glaze thickness being between 0.001 inch and 0.005 inch.

During the high power test on the disc, the Geiger Counter again registered only background radiation. This time, however, a blue glow-discharge was visible in the back chamber of the cavity. The discharge was first noticeable at about 250 Kw and increased in brightness as the power level was raised. Between 1000 Kw and 1200 Kw the magnetron misfired repeatedly and sparking occurred within the cavity.

On dismantling the cavity, no major breakdown was visible on either the glazed or unglazed surface of the disc. There was one small track of reduced ceramic originating at the edge of the disc, on the glazed side. The removal of the copper supporting ring revealed extensive breakdown along the disc perimeter. The discolouration occurred in areas where the disc had made imperfect contact with the ring.

3.4 Breakdown Test IV - Glazed Disc With Thin Aluminum Edge-Coating.

The glaze on the disc surface was dissolved in nitric acid. The reduced area was restored to titania ceramic by heating the disc to 850°C in an oxidizing atmosphere, and allowing it to cool gradually. One side of the disc was then reglazed.

The presence of edge breakdown, even in the theoretical absence of strong E fields at the edge of the disc, was somewhat surprising and it was decided to investigate the use of a metal film on the disc edge. Such a coating provides a more uniform metal-ceramic bond than is possible with only the disc and metal ring. Many metals are suitable for this purpose but aluminum was chosen for the relative ease with which it is possible to evaporate, onto a surface, a homogeneous layer of uniform thickness.

The disc was placed in an evacuated jar. It was supported about 4 inches above a tungsten filament around which was wound a thin strip of aluminum. When the pressure reached 10^{-4} mm Hg or below, current was supplied to the filament and the aluminum evaporated, a small portion adhering to the ceramic edge. The disc was then rotated and a new aluminum charge was placed on the filament. This procedure was repeated until the entire circumference of the disc was coated. The final resistance of the aluminum

film, as measured across the diameter of the disc, was 70 ohms. This resistance represents a film thickness much less than one skin depth of aluminum at 3000 mcs.

The experimental procedure was the same as in the previous high power tests. Again, the peak power was 1.2 Mw, there was no significant radiation, and a blue glow discharge was evident in the back chamber. Subsequent inspection of the disc revealed a large tree-like pattern of reduced ceramic on the back face of the disc. The breakdown occurred near the circumference and was linked to the edge of the disc by a breakdown track originating at the metal-ceramic contact. There were a number of small pits in the titania surface within the reduced area. The cavity end wall, opposite the breakdown, was discoloured by the same type of concentric rings that were observed in the first and second high power tests.

There was evidence, on the disc edge, of some sparking between the aluminum film and the copper supporting ring. Isolated areas of reduced titania were present in regions of imperfect metal-ceramic contact. This edge breakdown, however, was much less severe than in the previous test.

The aluminum remained completely bonded to the ceramic, even in the regions where sparking was most evident. In high power experiments reported by R. Hayes[10]

an edge coating of silver was stripped from the ceramic and deposited on the inside of the copper ring.

Figures 3.5 and 3.6 illustrate the breakdown.

3.5 Breakdown Test V - Glazed Disc With Improved Aluminum Edge-Coating.

The disc was prepared as described in section 3.4. For this test, however, a much thicker coating of aluminum was placed on the disc edge. The total resistance across the diameter was reduced to about 2 ohms. The actual thickness of the film was of the order of $\frac{1}{2}$ the skin depth of aluminum at 3000 mcs.

Instead of the Geiger Counter, which failed to indicate breakdown in previous tests, an ion guage was used to monitor the breakdown. The guage was mounted over the probe hole and was made vacuum tight with an "O" ring seal. A sudden pressure increase, as a result of ionization during breakdown, registers on the ion guage and provides a means of determining the power level at which a breakdown in the back chamber occurs.

The disc was thoroughly degreased and placed in the cavity. The system was pumped until the pressure in the waveguide run was 2×10^{-6} mm Hg; the back chamber pressure was about 10^{-4} mm Hg. During the outgassing process each jump in back chamber pressure was indicated on the ion guage. Once the system was outgassed, no further pressure change was recorded. The maximum power level for

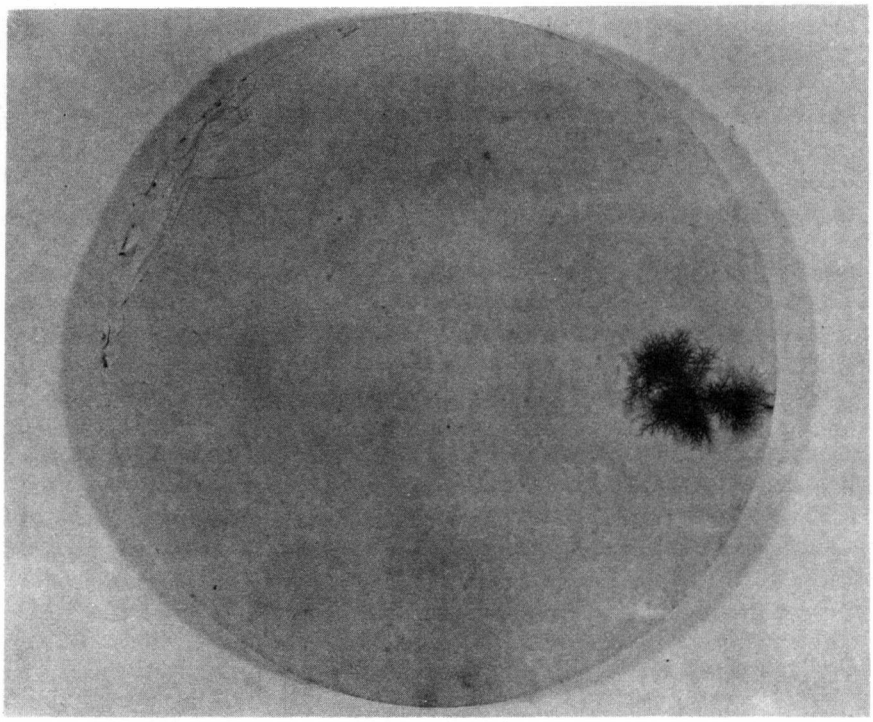

Fig. 3.5 Ceramic Breakdown - Test IV

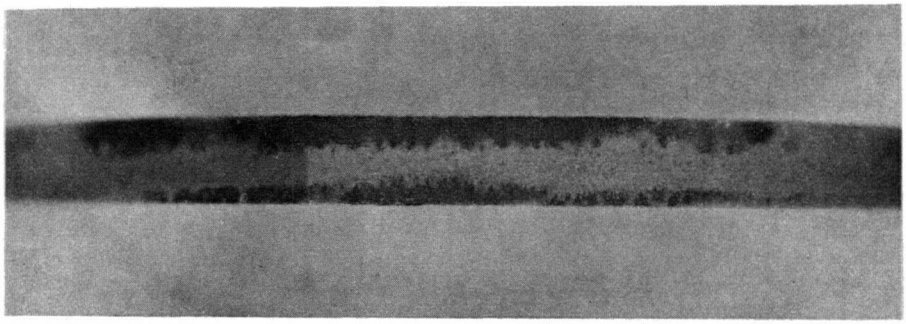

Fig. 3.6 Edge Breakdown - Test IV

this test was 1.6 Mw. At the 1 Mw level, power was delivered continuously for a 30 minute period.

Dismantling the cavity revealed only a light brown stain on both sides of the disc. The discolouration was in the form of a 'smoke-ring' about the centre of the disc, the average radius being between 1.8 and 1.9 cm. There were no areas of reduced titania anywhere on the disc surface.

Inspection of the disc with the copper ring removed showed only two isolated areas where a weak discharge had occurred between the aluminum and the copper. Again, there were no signs of the aluminum pealing from the ceramic edge.

3.6 Discussion of Results.

The heating of the cavity in the first two tests indicated that a large amount of power was dissipated in the disc, producing the extensive region of reduced titania. This heating is also a possible explanation of the coloured concentric rings on the end plate since heating brass produces similar effects to those observed. In this case, however, any heating effect on the end plate would have produced a distorted pattern because of the presence of the coupling hole. No such distortion existed, and it is far more probable that the coloured rings were due to the deposition of a thin film on the

end plate. Variations in film thickness would produce the coloured rings. The pitting at the ceramic surface suggests that material was evaporated from the disc during breakdown and deposited on the end plate.

The breakdown probably occurred at a relatively low power level as a result of sparking at the surface; the sparking being initiated by contamination or some intrinsic weakness due to surface condition or material composition. The sparking reduced the titania to a lower semiconducting oxide that then dissipated power and heated the disc. The heating further reduced the titania, leading to more dissipation and a greatly reduced cavity Q_o.

The coupling fields could also have played an important part in this first breakdown. In the back chamber the pure mode should exist because, in terms of wavelength, it is well removed from the coupling hole. The same is not true for the front chamber. An appreciable axial E field can exist due to the coupling hole, and this field, in conjunction with the possibility of field emission from the sharp edges of the iris, could initiate a breakdown at the ceramic. The coupling hole is undoubtedly prone to field emission because the final diameter was reached by hand reaming; the result being a scalloped effect around the hole circumference.

The above discussion strongly indicates that the

breakdown was not solely dependent on an E field tangential to the disc surface. For this reason the low power level at which breakdown occurred does not yield a true indication of the surface breakdown potential of a titania disc.

For the third test, with the glaze inhibiting the breakdown on the front face of the disc, it is reasonable to assume that the fields within the cavity increased until the next most vulnerable portion of the disc failed. The assumption of higher fields is also supported by the presence of the glow discharge in the back chamber. The discharge was the result of ionization of the low pressure air in the cavity. Since for all tests the pressure was of the same order of magnitude, the discharge indicates higher field strengths in the third test than in the first two tests.

This increased power level caused breakdown at the disc edge. Theoretically, the E field is zero at the disc edge and edge breakdown should not occur. However, surface irregularities and losses in the walls will produce finite fields at the disc perimeter. These fields can be enhanced by as much as a factor of ε_r (93 for titania), and can cause field emission in gaps at the metal-ceramic contact. The resulting sparking can cause breakdown at the titania edge. Trapped pockets of air with relatively low breakdown strengths could also cause

sparking, initiating breakdown at the ceramic.

The aluminum film used in test IV greatly reduced the edge breakdown by providing a uniform metal-ceramic contact. The fields were further increased, to the point where a major breakdown occurred on the back surface of the disc. The breakdown mechanisms described in conjunction with tests I and II were probably also responsible for the surface breakdown in test IV, although this time it appears that the initial heating and sparking was associated with the edge of the disc.

The final test establishes that the surface breakdown strength of titania is much higher than has been measured in previous experiments. R. Hayes[10] has shown that at radial E fields of between 6 and 14 $\frac{Kv}{cm}$ titania discs will fail because of edge effects. In test V, with edge breakdown almost completely suppressed, the E field strength was increased to well over 50 $\frac{Kv}{cm}$, and no breakdown occurred.

Two conclusions may be drawn:

(i) The surface breakdown strength of titania in the presence of a tangential E field is significantly higher than has been measured when edge effects have initiated breakdown. This result implies that, properly handled, titania can be successfully employed in high

power microwave devices.

(ii) The aluminum film substantially improves the edge breakdown strength of the titania discs, and it does not peel from the surface at high r.f. power levels.

4. ELECTRON MOTION IN THE S-BAND CAVITY

4.1 Introduction.

The presence of sufficiently energetic electrons, in conjunction with the applied electromagnetic field, can initiate breakdown at a dielectric surface.

When electrons impinge on the surface most of their energy is lost in exciting electrons in the dielectric. This excitation can result in bringing electrons from the valence band to the conduction band, some with sufficient mobility to reach the surface and escape. The amount of this secondary emission and the surface conductivity govern the magnitude of local surface charging which can produce high voltage gradients, possibly resulting in electrical discharges. In addition to increased conductivity and surface charging, sustained bombardment, by an electron resonance or multipactor effect, can cause local heating intense enough to chemically reduce the dielectric surface.

The present discussion is concerned with the motion of electrons emitted from the dielectric surface, with emphasis on determining upper limits to electron energies. R. Hayes[10] concluded that titania could withstand bombarding energies up to 10 Kev without structural damage, hence, such upper limits are useful in assessing the part played by electron bombardment in the breakdown, as well as in explaining the complete absence of any

detectable X-radiation during the high power tests.

4.2 Approximate Numerical Solution by Method of Runge-Kutta.

The classical equations of motion, derived from the force equation

$$\frac{m d\bar{V}}{dt} = e\bar{E} + e\bar{V} \times \bar{B}$$

and expressed in cylindrical coordinates, as given by W.H. Hayt[18] are:

$$\ddot{r} - r(\dot{\theta})^2 = \frac{e}{m}(E_r + B_z \omega r - B_\theta \dot{z})$$

$$\frac{1}{r}\frac{d}{dt}(r^2\dot{\theta}) = \frac{e}{m}(E_\theta + B_r \dot{z} - B_z \dot{r}) \qquad \ldots 4.1$$

$$\ddot{z} = \frac{e}{m}(E_z + B_\theta \dot{r} - B_r \omega r)$$

where the appropriate cavity fields are:

$$H_z = -H_1 J_o(kr)\sinh\alpha z . e^{j\omega t}$$

$$H_r = \frac{\alpha}{k} H_1 J_1(kr)\cosh\alpha z . e^{j\omega t} \qquad \ldots 4.2$$

$$E_\theta = \frac{j\omega\mu_1}{k} H_1 J_1(kr)\sinh\alpha z . e^{j\omega t}$$

where $\mu = \mu_1 = \mu_o \cong 4\pi \times 10^{-7} \frac{h}{m}$.

A solution was attempted by neglecting the H fields and limiting the possible initial values of r to $0.0184 \leq r_o \leq 0.0385$ metres. In this range $J_1(kr)$ was approximated as $\frac{11.5 \times 10^{-3}}{r}$. An arbitrary level of $E_{\theta max} = 29 \frac{Kv}{cm}$ was used, and the time variation was suppressed. The following equations resulted:

$$\ddot{r} - r\dot{\theta}^2 = 0$$

and ...4.3

$$\frac{d}{dt}(r^2\dot{\theta}) = 10^{16}$$

The numerical method of Runge-Kutta was used and a solution for the trajectory of an electron emitted at $r_o = 0.0184$ m was obtained. The time the electron remained in the field, was approximately 4×10^{-10} sec. which is comparable to one cycle at 3000 mc, hence, the suppression of $e^{j\omega t}$ was not justified.

Two further solutions were obtained including the time dependence, assuming $t_o = 0$ and $t_o = T/4$, where T is the period, and $r_o = 0.0184$. Figure 4.1 shows the resulting trajectories.

The velocities obtained, assuming no H fields, when substituted into $\bar{F} = e\bar{V} \times \bar{B}$, showed that the magnetic contribution was not negligible. In fact, the resulting velocity in the z-direction was comparable to

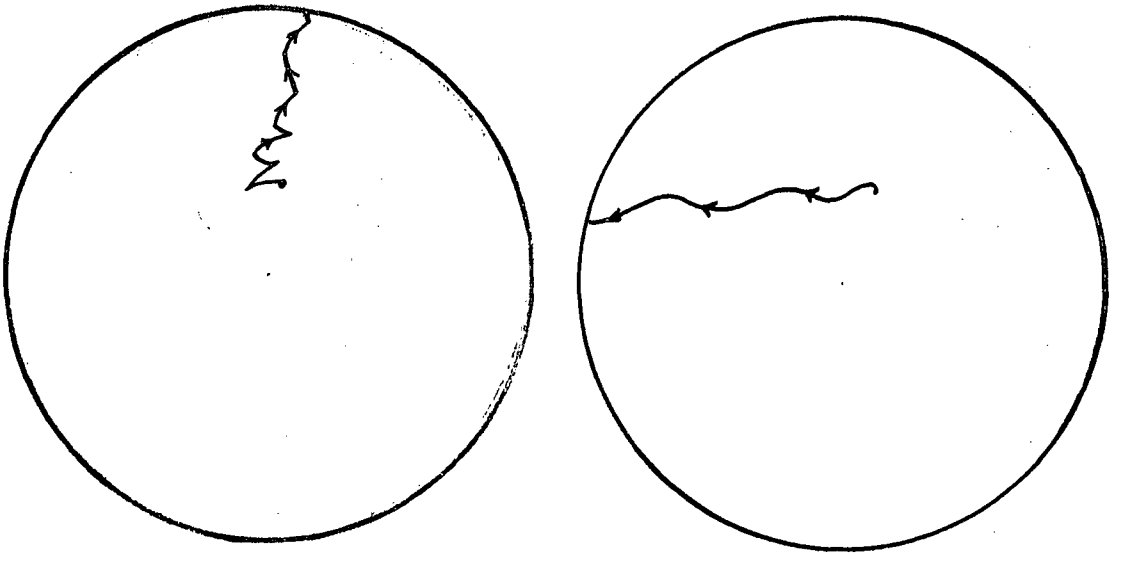

Fig. 4.1 Typical Trajectories

the radial velocity. Also, these numerical solutions yielded no generalized energy information and another method based on the Hamiltonian of the motion was used.

4.3 Potential Expressions for Cavity Fields.

In order to use the Hamiltonian approach to electron dynamics, it is necessary to know the scalar and vector potentials representing the field quantities. Let $\bar{A}$ be the vector potential and V be the scalar potential, then:

$$\mu\bar{H} = \text{curl } \bar{A} \qquad \ldots 4.4$$

$$\bar{E} = -\text{grad } V - \dot{\bar{A}}$$

The cavity fields are as given in section 4.2.

Hence

$$\bar{i}_r \cdot \frac{\mu\alpha}{k} H_1 J_1(kr)\cosh\alpha z \cdot e^{j\omega t} - \bar{i}_z \cdot \mu H_1 J_0(kr)\sinh\alpha z e^{j\omega t} =$$

$$\left[\frac{1}{r}\frac{\partial A_z}{\partial \theta} - \frac{\partial A_\theta}{\partial z}\right]\bar{i}_r + \left[\frac{1}{r}\frac{\partial rA_\theta}{\partial r} - \frac{1}{r}\frac{\partial A_r}{\partial \theta}\right]\bar{i}_z$$

and

$$\bar{i}_\theta \cdot \frac{j\omega\mu}{k} H_1 J_1(kr)\sinh\alpha z \cdot e^{j\omega t} = \bar{i}_\theta(-j\omega A_\theta) - \bar{i}_\theta \cdot \frac{1}{r}\frac{\partial V}{\partial \theta}$$

A solution of these equations gives:

$$\bar{A} = \frac{-B_1}{k} J_1(kr)\sinh\alpha z e^{j\omega t} \cdot \bar{i}_\theta \quad \ldots 4.5$$

$$V = 0$$

where

$$B_1 = \mu_o H_1$$

4.4 The Hamiltonian and the Equations of Motion

The cavity fields reduce to a single vector potential $\bar{A} = \frac{B_1}{k} J_1(kr)\sinh\alpha z \begin{matrix}\sin\omega t \\ -\cos\omega t\end{matrix} \bar{i}_\theta$.

The Hamiltonian of the motion, when expressed in terms of $\bar{P}$, the vector canonic momentum, and the scalar and vector potentials, is given as[20]:

$$\mathcal{H} = \frac{1}{2m}\left[\bar{P} - e\bar{A}\right]^2 + eV$$

where e is the charge. Substituting for $\bar{P}$ and $\bar{A}$

$$\mathcal{H} = \frac{1}{2m}\left[P_r^2 + \frac{1}{r^2}\left\{P_\theta - er\,\frac{B_1}{k}J_1(kr)\sinh\alpha z \begin{matrix}\sin\omega t \\ -\cos\omega t\end{matrix}\right\}^2 + P_z^2\right] \qquad \ldots 4.6$$

The equations of motion are obtained from $\mathcal{H}$ via the canonic equations of Hamilton:

$$\dot{q}_i = \frac{\partial \mathcal{H}}{\partial P_i} \qquad \text{and} \qquad -\dot{P}_i = \frac{\partial \mathcal{H}}{\partial q_i} \qquad \ldots 4.7$$

where $q_1 = r$, $q_2 = \theta$, $q_3 = z$.

Hence:

(1) $\dot{r} = \frac{P_r}{m}$

(2) $\dot{\theta} = \frac{P_\theta}{mr^2} - \frac{eB_1}{km} \cdot \frac{J_1(kr)}{r} \sinh\alpha z \begin{matrix}\sin\omega t \\ -\cos\omega t\end{matrix}$

(3) $\dot{z} = \frac{P_z}{m}$

(4) $\dot{P}_r = -\frac{\partial}{\partial r}\left[\frac{1}{2m}\left\{\frac{P_\theta}{r} - \frac{eB_1}{k} J_1(kr)\sinh\alpha z \begin{matrix}\sin\omega t \\ -\cos\omega t\end{matrix}\right\}^2\right]$ $\qquad \ldots 4.8$

(5) $\dot{P}_\theta = 0$ and P_θ = constant

$$(6)\quad \dot{P}_z = \frac{-\partial}{\partial z}\left[\frac{1}{2m}\left\{\frac{P_\theta}{r} - \frac{eB_1}{k} J_1(kr)\sinh\alpha z \begin{matrix}\sin\omega t \\ -\cos\omega t\end{matrix}\right\}^2\right]$$

Manipulating equations 4.8 and making a time-average approximation, as will be done in subsequent sections, yields:

$$\ddot{z} = \frac{-\partial}{\partial z}\left[\left(\frac{eB_1}{km}\right)^2 \frac{J_1{}^2(kr)}{4} \sinh^2\alpha z\right] \qquad \ldots 4.9$$

Thus, $\ddot{z}$ is an acceleration away from the surface of the disc, towards regions of weaker E field, and the final electron energies will be smaller than if the motion had been confined to the plane of the disc. Upper limits to transverse velocities, therefore, can be obtained by eliminating the z-dependence of $\bar{A}$, thereby confining the electrons to the transverse plane. Sections 4.5 and 4.6 utilize this simplification.

4.5 Electron Emitted at Instant of Maximum E_θ-Time-Average Approximation.

The z-independent vector potential becomes:

$$A_\theta = \frac{B_1}{k} J_1(kr)\sin\omega t \qquad \ldots 4.10$$

and

$$\dot{\theta} = \frac{P_\theta}{mr^2} - \frac{eB_1}{km} \cdot \frac{J_1(kr)}{r} \sin\omega t \qquad \ldots 4.11$$

$$\dot{P}_r = \frac{\partial}{\partial r}\left[\frac{1}{2m}\left\{\frac{P_\theta}{r} - \frac{eB_1}{k} J_1(kr)\sin\omega t\right\}^2\right]$$

The problem is further specified by the initial conditions. Assume $\dot{\theta} = o$, $r = r_o$ at $t = t_o = o$. Equations 4.11 show that for this case, $P_\theta = o$, and:

$$\dot{P}_r = \frac{-\partial}{\partial r}\left[\left(\frac{eB_1}{k}\right)J_1(kr)\sin\omega t\right]^2 \cdot \frac{1}{2m}$$

hence

$$\ddot{r} = \frac{-\partial}{\partial r}\left[\frac{1}{2}\left(\frac{eB_1}{km}\right)^2 J_1^{\,2}(kr)\sin^2\omega t\right] \quad \ldots 4.12$$

At this point the assumption is made that ωt varies rapidly enough to justify the use of the time-averaged acceleration, and $\sin^2\omega t$ is replaced by $\frac{1}{2}$. Therefore

$$\ddot{r} = \frac{-\partial}{\partial r}\left[\frac{1}{4}\left(\frac{eB_1}{km}\right)^2 J_1^{\,2}(kr)\right] = \frac{-\partial}{\partial r}\psi(r)$$

$$\dot{r}\ddot{r} = \frac{-\partial}{\partial r}\psi(r)\dot{r}$$

$$\frac{1}{2}\frac{d}{dt}\dot{r}^2 = \frac{-d}{dt}\psi(r)$$

$$\dot{r}^2 + 2\psi(r) = K_o, \text{ but } \dot{r} = 0 \text{ at } r = r_o$$

and

$$\dot{r}^2 + \frac{1}{2}\left(\frac{eB_1}{mk}\right)^2 J_1^{\,2}(kr) = \frac{1}{2}\left(\frac{eB_1}{mk}\right)^2 J_1^{\,2}(kr_o) \quad \ldots 4.13$$

Hence

$$\dot{r} = (K_o - 2\psi(r))^{\frac{1}{2}} = \frac{dr}{dt}$$

and

$$\sqrt{2}\left(\frac{mk}{eB_1}\right) \int \frac{dr}{\left[J_1^2(kr_o) - J_1^2(kr)\right]^{\frac{1}{2}}} = \int dt \qquad \ldots 4.14$$

The evaluation of this integral is simplified by linearizing $J_1^2(kr)$ over the range of interest, $0.0184 \leq r \leq 0.0385$ metres. A sufficiently accurate approximation is

$$J_1^2(kr) \cong 0.65 - 16.9r \qquad \ldots 4.15$$

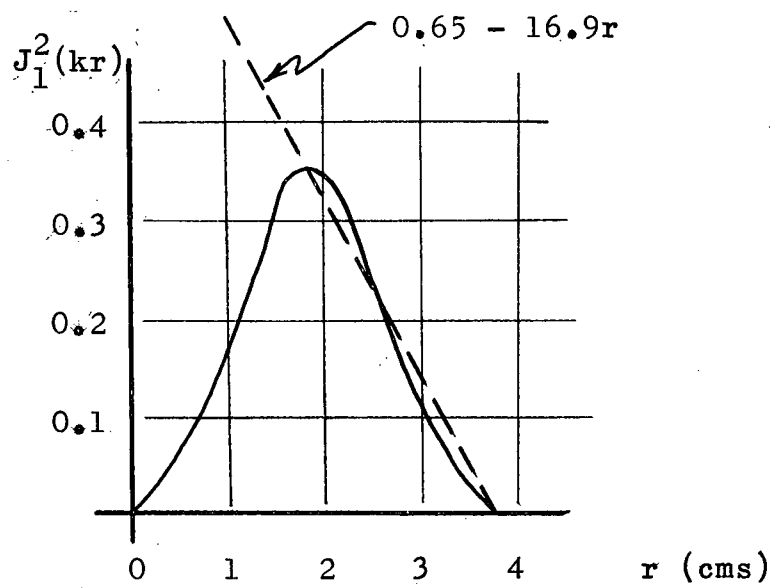

Fig. 4.2 $J_1^2(kr)$ Approximation

Figure 4.2 illustrates the nature of this approximation.

Substituting equation 4.15 in 4.14,

$$\sqrt{2}\left(\frac{mk}{eB_1}\right)\int \frac{dr}{\left[J_1^2(kr_o) - 0.65 + 16.9r\right]^{\frac{1}{2}}} = \sqrt{2}\left(\frac{mk}{eB_1}\right)\int \frac{dr}{(a + br)^{\frac{1}{2}}}$$

$$= \sqrt{2}\left(\frac{mk}{eB_1}\right)\frac{2}{16.9}\left[J_1^2(kr_o) - 0.65 + 16.9r\right]^{\frac{1}{2}}$$

Therefore

$$t \cong \sqrt{2}\left(\frac{mk}{eB_1}\right)\frac{2}{16.9}\left[16.9r - 0.31\right]^{\frac{1}{2}} \text{ for } r_o = 0.0184 \text{ metres} \quad \ldots 4.16$$

Now squaring both sides of equation 4.16 yields:

$$r(t) = 2.11\left(\frac{eB_1}{mk}\right)^2 t^2 + 0.0184 \quad \ldots 4.17$$

Referring back to equation 4.13 for $\dot{r}$, it is possible to establish an upper limit to the radial velocity.

$$\dot{r}^2 + \frac{1}{2}\left(\frac{eB_1}{mk}\right)^2 J_1^{\,2}(kr) = \frac{1}{2}\left(\frac{eB_1}{mk}\right)^2 J_1^{\,2}(kr_o)$$

Therefore at the cavity wall, $r = r_{max} = 0.0385$ m.

$$(\dot{r}^2)_{max} = \frac{1}{2}\left(\frac{eB_1}{mk}\right)^2 J_1^2(kr_o) \text{ as } J_1^2(kr) = 0$$

Hence

$$|\dot{r}| \leq \frac{1}{\sqrt{2}}\left(\frac{eB_1}{mk}\right) J_1(kr_o) \qquad \ldots 4.18$$

The radial velocity will be maximum when both $J_1(kr_o)$ and B_1 are maximum. B_1 is a maximum when the total available power of 2Mw is fed to the cavity, operating with $Q_o \cong 2000$, and $J_1(kr_o)$ is a maximum when $r_o = 0.0184$ m. $B_{1max} = 5.1 \times 10^4 \times \mu_o$.

Then

$$|\dot{r}| \leq 48 \times 10^6 \text{ m/s}$$

The tangential velocity component, $r\dot{\theta}$, is given as:

$$r\dot{\theta} = \left(\frac{eB_1}{km}\right) \cdot J_1(kr) \cdot \sin\omega t$$

and

$$|r\dot{\theta}| < \left(\frac{eB_1}{km}\right) J_1(kr_o) \qquad \ldots 4.19$$

For

$$r_o = 0.0184 \text{ m}, \; B_1 = \mu_o \times 5.1 \times 10^4$$

$$|r\dot{\theta}| < 67 \times 10^6 \text{ m/s}$$

In the actual resonant cavity there will also be an axial component of velocity, $\dot{z}$, since the fields are

dependent on z. Equation 4.9 enables an estimate to be made of $\dot{z}$.

$$\ddot{z} = -\frac{\partial}{\partial z}\left[\left(\frac{eB_1}{km}\right)^2 \frac{J_1^2(kr)}{4} \sinh^2\alpha z\right] \quad \ldots 4.9$$

The solution of this equation is simplified by linearizing $\sinh^2\alpha z$ in such a fashion that $\ddot{z}$ is always greater than the actual $\ddot{z}$. This may be accomplished by taking $\sinh^2\alpha z \cong 107z$ for $0 \leq \alpha z \leq 1$.

Therefore

$$\ddot{z} \cong \frac{-107}{4}\left(\frac{eB_1}{km}\right)^2 J_1^2(kr), \quad J_1^2(kr) = 0.65 - 16.9r$$

$$\ddot{z} \cong -26.8\left(\frac{eB_1}{km}\right)^2\left[0.65 - 16.9r\right]$$

From equation 4.17,

$$\ddot{z} \cong -26.8\left(\frac{eB_1}{km}\right)^2\left[0.34 - 35.7\left(\frac{eB_1}{mk}\right)^2 t^2\right]$$

$$\dot{z} \cong -26.8\left(\frac{eB_1}{km}\right)^2\left[0.34t - 11.9\left(\frac{eB_1}{mk}\right)^2 t^3\right] + C \quad \ldots 4.20$$

but $\dot{z} = 0$, $t = t_o = 0$, therefore $C = 0$

Hence

$$z \cong -26.8\left(\frac{eB_1}{km}\right)^2\left[0.17t^2 - 2.98\left(\frac{eB_1}{km}\right)^2 t^4\right] + .0129 \quad \ldots 4.21$$

Inspection of equation 4.21 indicates that the transit time of the electron from the disc to the cavity end wall is, $t_r < 5 \times 10^{-10}$ sec, and referring to equation 4.20:

$$|\dot{z}| < 45.5 \left(\frac{eB_1}{km}\right)^2 \times 10^{-10} \qquad \ldots 4.22$$

$$|\dot{z}| < 58 \times 10^6 \text{ m/s}$$

The terminal velocity, $\overline{U}_T$, of the electrons can be obtained by the vector sum of the component velocities. Thus

$$|\overline{U}_T| < (58^2 + 48^2)^{\frac{1}{2}} \times 10^6$$

$$|\overline{U}_T| < 75.2 \times 10^6 \text{ m/s}$$

Equating energies

$$eV = \frac{1}{2} m |\overline{U}_T|^2$$

and

$$V = \frac{75.2 \times 75.2 \times 10^{12}}{5.93 \times 5.93 \times 10^{10}} \cong 16000 \text{ volts.}$$

Hence, the terminal energy of an electron emitted from the disc at an instant when the E_θ field is a

maximum is less than 16.0 Kev.

4.6 Electron Emitted at Instant of Minimum E_θ-Time-Average Approximation.

Consider the electron released at $t_o + \frac{T}{4}$, which implies that:

$$A_\theta = \frac{-B_1}{k} J_1(kr)\cos\omega t$$

Therefore

$$\dot{\theta} = \frac{P_\theta}{mr^2} + \left(\frac{eB_1}{km}\right) \frac{J_1(kr)}{r}\cos\omega t$$

$$\dot{P}_r = \frac{-\partial}{\partial r}\left[\frac{1}{2m}\left\{\frac{P_\theta}{r} + \frac{eB_1}{k} J_1(kr)\cos\omega t\right\}^2\right] \quad \ldots 4.23$$

$$\dot{r} = \frac{P_r}{m}$$

and

$$\ddot{r} = \frac{P_\theta^2}{m^2 r^3} - \frac{\partial}{\partial r}\left[\left(\frac{eB_1}{km}\right)^2 \frac{J_1^2(kr)}{2}\cos^2\omega t + \frac{P_\theta}{m}\cdot\frac{eB_1}{km}\cdot\frac{J_1(kr)}{r}\cos\omega t\right]$$

where

$$P_\theta = -\left(\frac{eB_1}{k}\right) r_o J_1(kr_o), \text{ from } \dot{\theta} = \quad \text{at } t = t_o = 0.$$

Again take the time-average of $\ddot{r}$. Note, however, that in this case the approximation is not as good as before because of the $\cos\omega t$ term appearing in $\ddot{r}$.

Thus

$$\ddot{r} = \frac{P_\theta^2}{m^2 r^3} - \frac{\partial}{\partial r}\psi(r), \quad \psi(r) = \frac{1}{4}\left(\frac{eB_1}{km}\right)^2 J_1^2(kr) \qquad \ldots 4.24$$

$$\dot{r}\ddot{r} = \frac{\dot{r}P_\theta^2}{m^2 r^3} - \dot{r}\frac{\partial}{\partial r}\psi(r)$$

and

$$\dot{r}^2 + \frac{P_\theta^2}{m^2 r^2} + 2\psi(r) = K_o$$

Substituting for $r = r_o$, $\dot{r}^2 = 0$ at $t_o = 0$.

$$K_o = \frac{P_\theta^2}{m^2 r_o^2} + \frac{1}{2}\left(\frac{eB_1}{km}\right)^2 J_1^2(kr_o) = \frac{3}{2}\left(\frac{eB_1}{km}\right)^2 J_1^2(kr_o)$$

and

$$\dot{r}^2 = \frac{3}{2}\left(\frac{eB_1}{km}\right)^2 J_1^2(kr_o) - \frac{1}{2}\left(\frac{eB_1}{km}\right)^2 J_1^2(kr) - \left(\frac{eB_1}{km}\right)^2 \frac{r_o^2}{r^2} J_1^2(kr_o) \qquad \ldots 4.25$$

$$\int \frac{dr}{\left[\frac{3}{2}\left(\frac{eB_1}{km}\right)^2 J_1^2(kr_o) - \frac{1}{2}\left(\frac{eB_1}{km}\right)^2 J_1^2(kr) - \left(\frac{eB_1}{km}\right)^2 \frac{r_o^2}{r^2} J_1^2(kr_o)\right]^{\frac{1}{2}}} = \int dt \qquad \ldots 4.26$$

Using equation 4.15 and $\frac{1}{r^2} = 0.57 \times 10^4 - 14.8 \times 10^4 r$ for $0.0184 \leq r \leq 0.0385$ metres, equation 4.26 becomes:

$$r = 6.36\left(\frac{eB_1}{km}\right)^2 t^2 + 0.0184 \qquad \ldots 4.27$$

As in Section 4.5 $\dot{r}$ is a maximum when $r_o = 0.0184$ m, $B_1 = \mu_o \times 5.10 \times 10^4 \ \frac{\text{webers}}{m^2}$ and $r_{max} = 0.0385$ m, the cavity wall.

Hence

$$\dot{r}^2_{max} = \frac{3}{2}\left(\frac{eB_1}{mk}\right)^2 J_1^2(kr_o) - \frac{P_\theta^2}{m^2 r_{max}^2}$$

Therefore

$$|\dot{r}| \leq \left[\frac{3}{2}\left(\frac{eB_1}{mk}\right)^2 J_1^2(kr_o) - \left(\frac{eB_1}{mk}\right)^2 J_1^2(kr_o)\left(\frac{r_o}{r_{max}}\right)^2\right]^{\frac{1}{2}} \qquad \ldots 4.28$$

and

$$|\dot{r}| \leq 75 \times 10^6 \text{ m/s}$$

The tangential velocity can be found from equations 4.23 as:

$$r\dot{\theta} = \frac{-eB_1}{mk} \cdot \frac{r_o}{r} \cdot J_1(kr_o) + \left(\frac{eB_1}{km}\right) J_1(kr)\cos\omega t$$

hence

$$|r\dot{\theta}_{max}| < 2\left(\frac{eB_1}{mk}\right) J_1(kr_o) \qquad \ldots 4.29$$

$$|r\dot{\theta}| < 132 \times 10^6 \text{ m/s}$$

The axial velocity can be approximated in the same fashion as in section 4.5, using equation 4.27.

$$\ddot{z} \cong -26.8\left(\frac{eB_1}{km}\right)^2\left[0.34 - 107.5\left(\frac{eB_1}{mk}\right)^2 t^2\right]$$

$$\dot{z} \cong -26.8\left(\frac{eB_1}{km}\right)^2\left[0.34t - 36\left(\frac{eB_1}{mk}\right)^2 t^3\right]$$

$$z \cong -26.8\left(\frac{eB_1}{km}\right)^2\left[0.17t^2 - 9\left(\frac{eB_1}{mk}\right)^2 t^4\right] + 0.0129$$

and $t_r \simeq 5 \times 10^{-10}$ sec.

$$|\dot{z}| < 35\left(\frac{eB_1}{km}\right)^2 \times 10^{-10} \qquad \ldots 4.30$$

$$|\dot{z}| < 44.5 \times 10^6 \text{ m/s}$$

Hence, the terminal velocity is given as:

$$|\dot{r}| \leq 75 \times 10^6 \text{ m/s}$$

$$|\dot{z}| \leq 44.5 \times 10^6 \text{ m/s}$$

$$|r\dot{\theta}_T| < 31.5 \times 10^6 \text{ m/s}$$

$$|\overline{U}_T| < (75^2 + 44.5^2 + 31.5^2)^{\frac{1}{2}} \times 10^6 \text{ m/s}$$

$$|\overline{U}_T| < 93 \times 10^6 \text{ m/s}$$

Hence

$$V = \left| \frac{93 \times 10^6}{5.93 \times 10^5} \right|^2 \cong 24{,}000 \text{ volts}$$

The terminal energy of an electron emitted from the disc at an instant when the E_θ field is a minimum is less than 25 Kev.

4.7 Estimation of Error Introduced by The Assumption of Time-Averaged Values.

Another approach to the solution of equations 4.8 is possible, that is to linearize $J_1^2(kr)$, $J_1(kr)$, $\frac{1}{r^3}$ before integration. The result is a linear differential equation with constant coefficients with the time dependence intact.

When reasonable linearizations are taken, an estimate of the maximum error associated with the time-average approximation is possible. Since the largest error will be associated with the motion discussed in Section 4.6, this case will be dealt with. Recalling equations 4.23,

$$\ddot{r} = \frac{P_\theta^2}{m^2 r^3} - \frac{\partial}{\partial r}\left[\left(\frac{eB_1}{km}\right)^2 \frac{J_1^2(kr)}{2} \cos^2\omega t + \frac{P_\theta}{m} \cdot \frac{eB_1}{km} \cdot \frac{J_1(kr)}{r} \cos\omega t \right]$$

The following linearizations are used:

$$\frac{1}{r^3} \cong 1.75 \times 10^5 - 4.17 \times 10^6 r$$

$$J_1^2(kr) \cong 0.65 - 16.9r$$

$$\frac{J_1(kr)}{r} \cong 60 - 1580r$$

where $0.0184 \leq r \leq 0.0385$m.

Therefore

$$\ddot{r} = \frac{P_\theta^2}{m^2} \times 1.75 \times 10^5 - \frac{P_\theta^2}{m^2} \times 4.17 \times 10^6 r + \frac{16.9}{2}\left(\frac{eB_1}{km}\right)^2 \cos^2\omega t$$

$$+ \frac{P_\theta}{m}\left(\frac{eB_1}{km}\right) 1580 \cos\omega t$$

Hence

$$r \cong 0.051 - 0.0326\cos\omega_r t - 0.575 \times 10^{-4}\cos 2\omega t$$

$$- 4.66 \times 10^{-4} \cos\omega t$$

$$\dot{r} \cong 81 \times 10^6 \sin\omega_r t + 2.5 \times 10^6 \sin 2\omega t + 10 \times 10^6 \sin\omega t$$

Time-averaging corresponds to dropping terms in (ωt) from r and $\dot{r}$. The resulting error is less than 3 percent in r and less than 16 percent in $\dot{r}$. Thus, to a reasonable degree of accuracy, time-average forces can be used.

4.8 Lorentz Time-Average Force.

A charged particle of either sign in a non-uni-

form field experiences an acceleration towards the position of smallest electric field strength. The acceleration is due to the time-averaged Lorentz force and is given by[21,22]:*

$$\bar{f} = \frac{-e^2}{4m\omega^2} \text{ grad } |\bar{E}|^2 \qquad \ldots 4.31$$

where e is the charge, m is the mass and $\bar{E}$ is the electric field vector.

The $\bar{E}$ field in the cavity is entirely transverse and given by:

$$E_\theta = \frac{j\omega\mu}{k} H_1 J_1(kr)\sinh\alpha z \cdot e^{j\omega t}$$

Hence

$$|E_\theta|^2 = \frac{\omega^2 B_1^{\,2}}{k^2} J_1^{\,2}(kr)\sinh^2\alpha z \qquad \ldots 4.32$$

From 4.31

$$\bar{f} = \frac{-e^2 B_1^{\,2}}{4mk^2}\left[\bar{i}_r\left\{\frac{\partial}{\partial r} J_1^{\,2}(kr)\sinh^2\alpha z\right\} + \bar{i}_\theta \frac{1}{r}\frac{\partial}{\partial\theta}\left\{J_1^{\,2}(kr)\sinh^2\alpha z\right\}\right.$$

$$\left. + \bar{i}_z \frac{\partial}{\partial z}\left\{J_1^{\,2}(kr)\sinh^2\alpha z\right\}\right]$$

$$= \frac{-e^2 B_1^{\,2}}{4mk^2}\left[\bar{i}_r \frac{\partial}{\partial r}\left\{J_1^{\,2}(kr)\sinh^2\alpha z\right\} + \bar{i}_z \frac{\partial}{\partial z}\left\{J_1^{\,2}(kr)\sinh^2\alpha z\right\}\right]$$

---

* See Appendix 1.

$$= \frac{-e^2 B_1^2}{2mk} \sinh^2 \alpha z J_1(kr) \left[J_o(kr) - \frac{1}{kr} J_1(kr) \right] \bar{i}_r$$

$$\frac{-e^2 B_1^2}{2mk^2} \alpha \sinh \alpha z \cosh \alpha z \, J_1^2(kr) \bar{i}_z \qquad \ldots 4.33$$

Thus, charged particles in the cavity experience a net force accelerating them away from the surface of the dielectric disc towards the cavity end wall. If the particles are released at $r_o > 0.0184$m, they will drift radially outwards and if $r_o < 0.0184$m, they will be accelerated towards the axis. Figure 4.3 illustrates the type of motion.

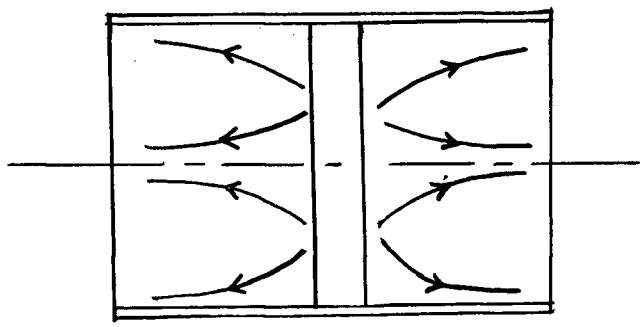

Fig. 4.3 Time-Averaged Electron Motion

4.9 Multipactor.

Secondary electron resonance effects, or multipactors, are of two basic types: two-surface, and single-surface, as recently proposed by Priest and Talcott[23].

The two-surface multipactor occurs when electrons from one surface are accelerated towards the second and arrive there at such a time that any secondaries emitted will be, in turn, accelerated towards the first surface. If the arrival energy of the electrons is within the range for which the secondary emission coefficient (δ) is greater than unity, the number of oscillating electrons will increase rapidly. The effect is critically dependent on the field, the gap length and the phase angle of the field at which an electron is emitted. In the present cavity it has been established that electrons will be accelerated away from the surface of the disc, and hence, a two-surface multipactor between the disc and end wall is virtually impossible.

Single-surface mutlipactor is dependent on free electrons 'dancing' on the surface. The electrons transfer energy from the field to the surface, causing more electrons to be released by secondary emission. Secondaries are initially carried away from the surface by their emission velocities but are returned by a restoring force due to surface charging or the presence of a tangential magnetic field. The test cavity has E and H field

components tangential to the surface. If an electron is emitted with a finite axial velocity at a time such that the H_r field produces a positive restoring force a multipactor could occur, provided that the total time the electron remains in the field is much less than one r.f. cycle. This time is given by $\frac{\pi m}{eB_1}$. In other words

$$\frac{\pi m}{eB_1} \ll 3.3 \times 10^{-10} \text{ sec.} \qquad \ldots 4.34$$

The inequality 4.34 would imply that $B = 10B_{max}$, where B_{max} is the maximum B_1 field possible in the cavity, and thus this type of multipactor is ruled out. If, on the other hand, the restoring force is due to a positive surface charge it is possible for the test cavity to sustain a single surface multipactor on the ceramic disc. This effect is possible over a wide range of field strengths which will enable the bombarding electrons to give $\delta > 1$.

4.10 Summary.

The foregoing analysis indicates that the following hypotheses and conclusions are valid:

1) The maximum energy of an electron striking any metal surface in the cavity is less than 25 Kev. Since the operating Q is less than the Q_o used in the calculations, and because the maximum power level for the high power tests is always less than the 2Mw peak, it is probable that the electron energies are not in excess of 10 Kev.

2) Bombarding energies of this order are not sufficient to give significant x-radiation external to the cavity.

3) Electrons experience a drift force away from the disc surface and hence it is not possible for them to return to the surface with high energies. As a result direct bombardment by energetic electrons does not have an important part in the observed breakdown.

4) There can be no two-surface multipactor, again because of the axial drift away from the disc surface.

5) A single-surface multipactor is possible with a positive surface charge. The resonance, however, is not self-starting. It requires the presence of a bombarding stream of electrons having energies that give $\delta > 1$, so as to build up the necessary positive charge. Such a stream is unlikely in the test cavity, and hence, while possible, this multipactor should not play a major role in the breakdown.

5. CONCLUSIONS

Ceramic breakdown at microwave frequencies, under the influence of purely tangential **E** fields, was investigated using an S-Band cavity operating in an H_{01} mode.

The discussion of electron motion in the cavity showed that electron energies were of the order of 10 Kev, and that the fields caused charged particles to drift away from the disc surface. Hence, electron bombardment and multipactor are not significantly important as breakdown mechanisms in this cavity, a fact that is supported by the absence of detectable X-radiation during the high power tests.

The series of high power tests showed that, by suppressing edge effects, particle bombardment, and multipactor, the surface breakdown strength of titania is greatly increased. The final test, using all available power, failed to cause breakdown of the titania. The E field, in this case, was in excess of 50 $\frac{Kv}{cm}$, a marked improvement over the 6 to 14 $\frac{Kv}{cm}$ measured by R. Hayes[10].

This significant increase in the power handling capabilities of the titania, in the H_{01} cavity, suggests the use of the H_{01} mode in other high power microwave applications. For example, high power microwave windows that commonly use the H_{11} mode could handle much higher

powers if they were designed to operate in the H_{01} mode.

The first aluminum film substantially reduced the edge breakdown and adhered well to the titania. Increasing the film thickness provided a further improvement. It is possible that, if the depth of the film is made greater than a skin depth, the edge problem can be eliminated, thus making complicated metal-ceramic brazes unnecessary.

The work undertaken in this thesis points out several topics for further investigation. These are:

(i) the study of a high power microwave window operating in an H_{01} mode,

(ii) the testing of the aluminum bond under the influences of radial and axial E fields, and

(iii) the investigation of thin metallic films on the surface of the ceramic.

APPENDIX 1: LORENTZ-TIME-AVERAGED FORCE

The Lorentz force on an electron is

$$\bar{f} = e(\bar{E}_e - \bar{V} \times \bar{B}_e) \qquad \ldots(1)$$

where $\bar{E}_e$, $\bar{B}_e$ are the time varying fields at the instantaneous position of the electrons.

Assume:

(i) that the electron motion is such that over one r.f. cycle the electron sees a nearly uniform field.

(ii) that the motion will be oscillatory with angular frequency approximately ω, the angular frequency of the fields.

The fields can be rewritten in terms of a displacement, $\Delta\bar{r}$, from the equilibrium position where the fields are respectively $\bar{E}_o$ and $\bar{B}_o$. Equation (1) becomes:

$$\bar{f} = e\left[\bar{E}_o + (\Delta\bar{r}\cdot\nabla)\bar{E}_o\right] + e\bar{V}x\left[\bar{B}_o + (\Delta\bar{r}\cdot\nabla)\bar{B}_o\right] \ldots(2)$$

$$= \bar{f}_1 + \bar{f}_2$$

If to a first order the term $\bar{V} \times \bar{B}_e$ can be neglected, $\bar{a} = \frac{e}{m}\bar{E}_e$ and $\bar{E}_e \approx \bar{E}_o$ where $\bar{a}$ is the acceleration

and $\bar{E}_o = \bar{E}e^{j\omega t}$.

Then

$$\bar{a} = \frac{d^2\Delta\bar{r}}{dt^2} = \frac{e}{m}\bar{E}e^{j\omega t}$$

$$\frac{d\Delta\bar{r}}{dt} = \frac{e}{m\omega j}\bar{E}e^{j\omega t}$$

and

$$\Delta\bar{r} = \frac{-e}{m\omega^2}\bar{E}_o \qquad \ldots(3)$$

Substituting this result in equation (2) yields:

$$\bar{f}_1 = \frac{-e^2}{m\omega^2}(\bar{E}_o \cdot \nabla)\bar{E}_o + e\bar{E}_o \qquad \ldots(4)$$

Therefore

$$\bar{f}_1 = \frac{-e^2}{m\omega^2}\left[\frac{1}{2}\nabla(\bar{E}_o \cdot \bar{E}_o) - \bar{E}_o \times \nabla \times \bar{E}_o\right] + e\bar{E}_o$$

But

$$\nabla \times \bar{E}_o = -\frac{\partial \bar{B}_o}{\partial t}$$

Hence

$$\bar{f}_1 = \frac{-e^2}{m\omega^2}\left[\frac{1}{2}\nabla(\bar{E}_o \cdot \bar{E}_o) + \bar{E}_o \times \frac{\partial \bar{B}_o}{\partial t}\right] + e\bar{E}_o \qquad \ldots(5)$$

Considering $\bar{f}_2$ gives:

$$\bar{f}_2 = e(\bar{V} \times \bar{B}_o) + e\bar{V} \times (\Delta\bar{r} \cdot \nabla)\bar{B}_o$$

but $\bar{V} = \frac{\partial \Delta\bar{r}}{\partial t}$, and the second term is small compared to the first, hence:

$$\bar{f}_2 = \frac{-e^2}{m\omega^2} \frac{\partial \bar{E}_o}{\partial t} \times \bar{B}_o \qquad \ldots(6)$$

Therefore

$$\bar{f} = \frac{-e^2}{m\omega^2} \left[\frac{1}{2} \nabla(\bar{E}_o \cdot \bar{E}_o) + \frac{\partial}{\partial t}(\bar{E}_o \times \bar{B}_o) \right] + e\bar{E}_o \qquad \ldots(7)$$

Taking the time-average of this expression yields:

$$\bar{f} = -\frac{1}{4} \frac{e^2}{m\omega^2} \nabla |E|^2 \qquad \ldots(8)$$

This force is known as the Lorentz-time-averaged force.

REFERENCES

1. Jasberg, J. and Lebacqz, J.V., Advances in Vacuum Science and Technology, vol. 2, p. 667, 1958.

2. Lebacqz, J.V., Jasberg, J., Shaw, H.T., and Sonkin, S., Proc. I.E.E. part B, vol. 105, suppl. 11, p. 617, 1958.

3. Sperry Gyroscope Company (New York), Report No. NA-8240-8182-1 to 4, 1960, "Investigation of Microwave Window Failure Mechanisms and their Elimination".

4. Electrical and Musical Industries Ltd. (U.K.) Report No. RF/271, 1960.

5. Preist, D.H. and Talcott, R.C., American Ceramic Soc. Bull., vol. 38, p. 99, 1959.

6. Walker, G.B. and Lewis, E.L., Nature, vol. 181, p. 38, 1958.

7. Walker, G.B. and Luthra, S.P., "Use of Ghost Modes to Determine Dielectric Constant and Loss Tangent", I.E.E. Conference on Microwave Measurement Techniques, Sept. 1961.

8. Walker, G.B., Report M.L. 2, Electrical Engineering, U.B.C., Nov. 1960.

9. Luthra, S.P., Ph.D. Thesis, University of London.

10. Hayes, R., "Phenomena Associated with Electrical Breakdown at Certain Dielectric Surfaces in Vacua", Report No. M.L. 4ECRDC Project T54, Sept. 1961.

11. Lamont, H.R.L., Waveguides, Methuen's Monograms, John Wiley and Sons, Inc., 1959.

12. Shnurer, F., "Design of Aperature-Coupled Filters", PGMTT, p. 238, Oct. 1957.

13. Bethe, H.A., "Lumped Constants for Small Irises", MIT RAD LAB R. No. 43-22, pp. 34-39.

14. Ramo, S. and Whinnery, H.R., Fields and Waves in Modern Radio, John Wiley and Sons, Inc., 1956.

15. Barlow, H.A. and Cullen, A.L., Microwave Measurements, p. 81, Constable and Company Ltd., 1950.

16. Gintzon, E.L., Microwave Measurements, McGraw Hill Company Inc., 1957.

17. Reich, H.J., Ordung, P.F., Krauss, H.L., and Skalnik, J.G., Microwave Theory and Techniques, p. 452, Van Nostrand, 1953.

18. Hayt, W.H., Engineering Electromagnetics, p. 295, McGraw Hill Co. Inc., 1958.

19. Hildebrand, F.B., Advanced Calculus For Applications, p. 102, Prentice-Hall, Inc., 1962.

20. Goldstein, H., Classical Mechanics, Addison-Wesley Publishing Company Inc., 1959.

21. Boot, H.A.H., Self, S.A., and R.-Shersbey-Harvie, R.B., J. Electronics and Control, vol. 4, p. 424, 1958.

22. Gapanov, A.V., and Miller, M.A., J. Exp. Theoret. Phys., vol. 7, p. 168, 1958.

23. Priest, D.H. and Talcott, R.C., I.R.E. Transactions E.D., vol. 8, p. 243, July 1961.